午後對流發展機制及診斷探討

楊明仁
台大大氣系

19 July 2018
Central Weather Bureau

Part I: Review of previous studies
(Lin et al. 2011; Lin et al. 2012; Chen et al. 2014)

Part II: A modeling study on the afternoon thunderstorm event at Taipei on 14 June 2015

46690: Danshui
46692: Taipei (Panchiao)
46694: Keelung
46699: Hualien
46748: Chiayi
46778: Chigu
46742: Yungkang

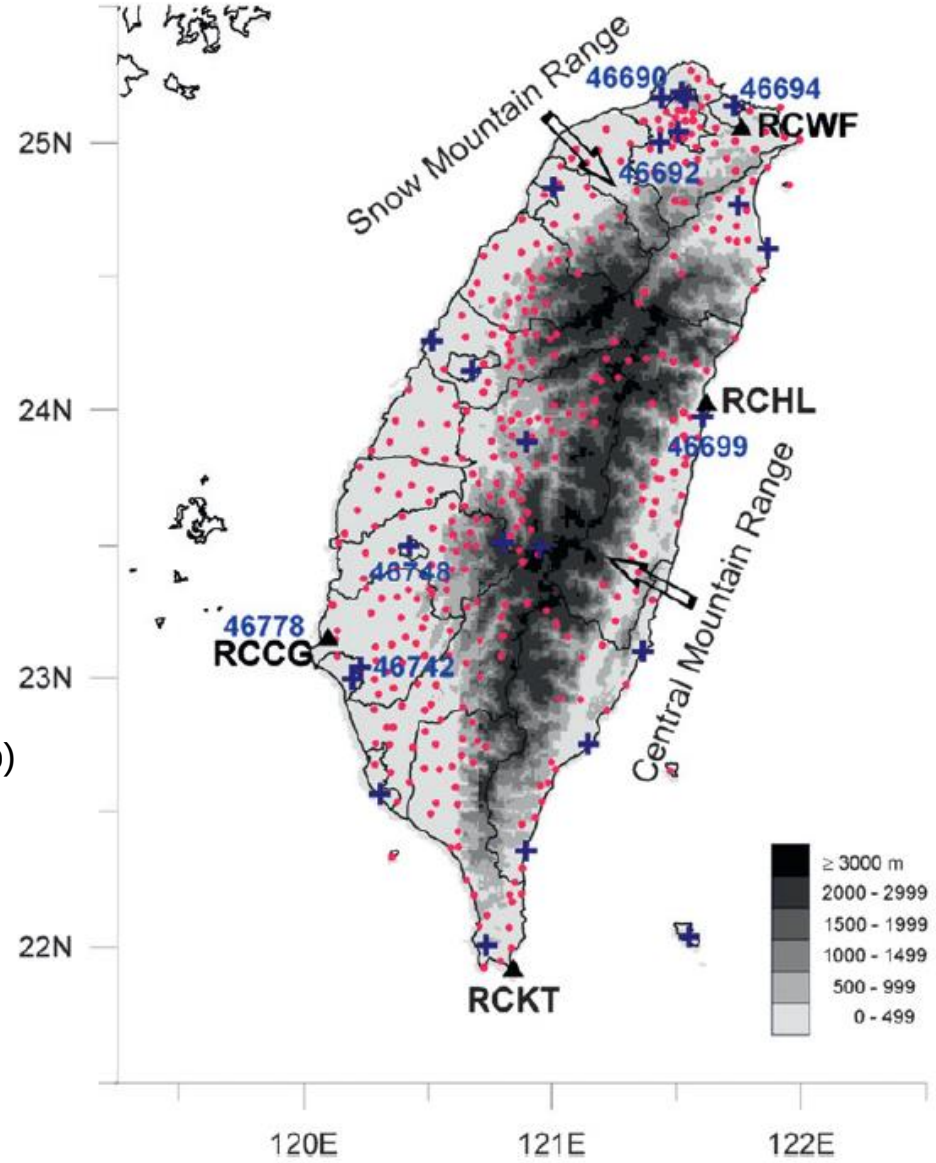

FIG. 1. Distributions of observation stations in Taiwan. Gray shades represent terrain heights. Locations of radar sites are marked with triangles and their respective abbreviations. Surface stations and rain gauges are denoted by blue plus signs and pink circles, respectively. Surface stations used in this study are labeled with the station numbers for reference.

Lin et al. (2011)

Warm season: May - October

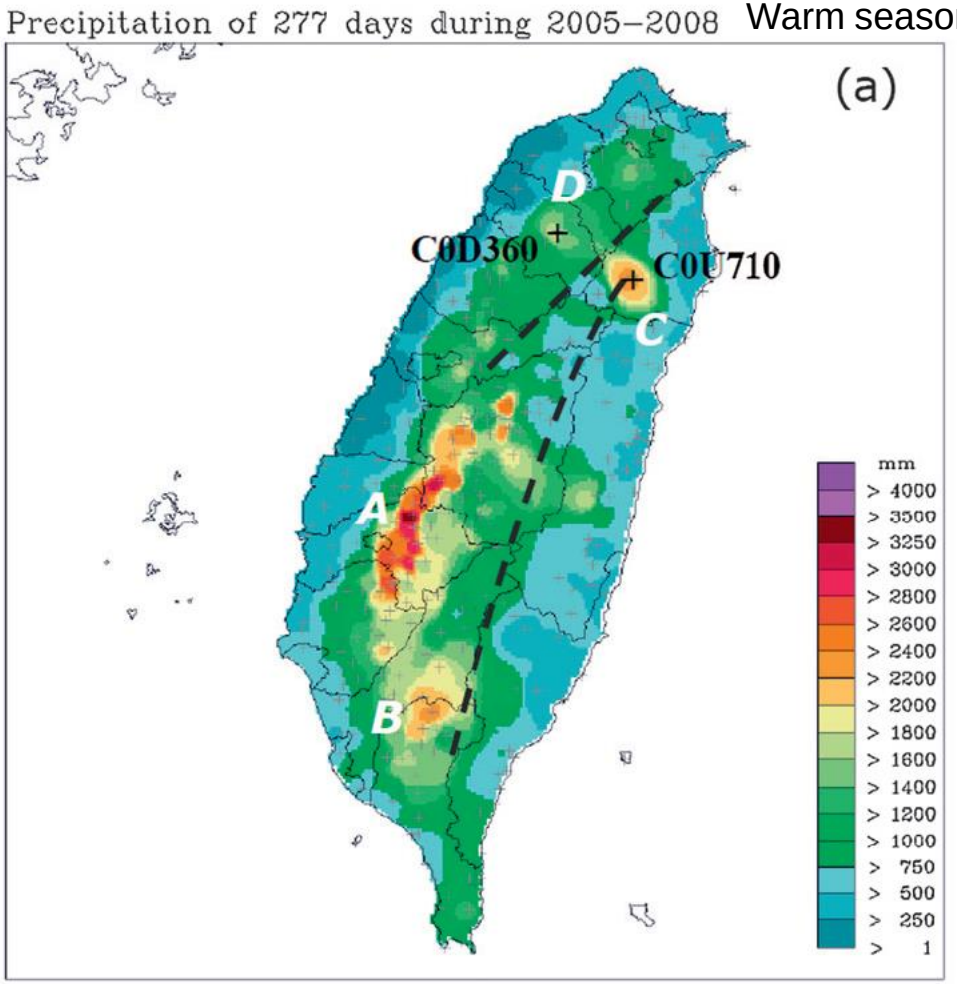

FIG. 2. (a) Distribution of rainfall amounts (mm) on undisturbed days during the warm seasons during 2005–08. Gauge stations with local precipitation maximum are labeled with the station numbers for reference. (b) Hourly average rainfall (mm) for all rain gauges. The dashed lines indicate the crest lines of two major mountain ranges (Fig. 1).

Lin et al. (2011)

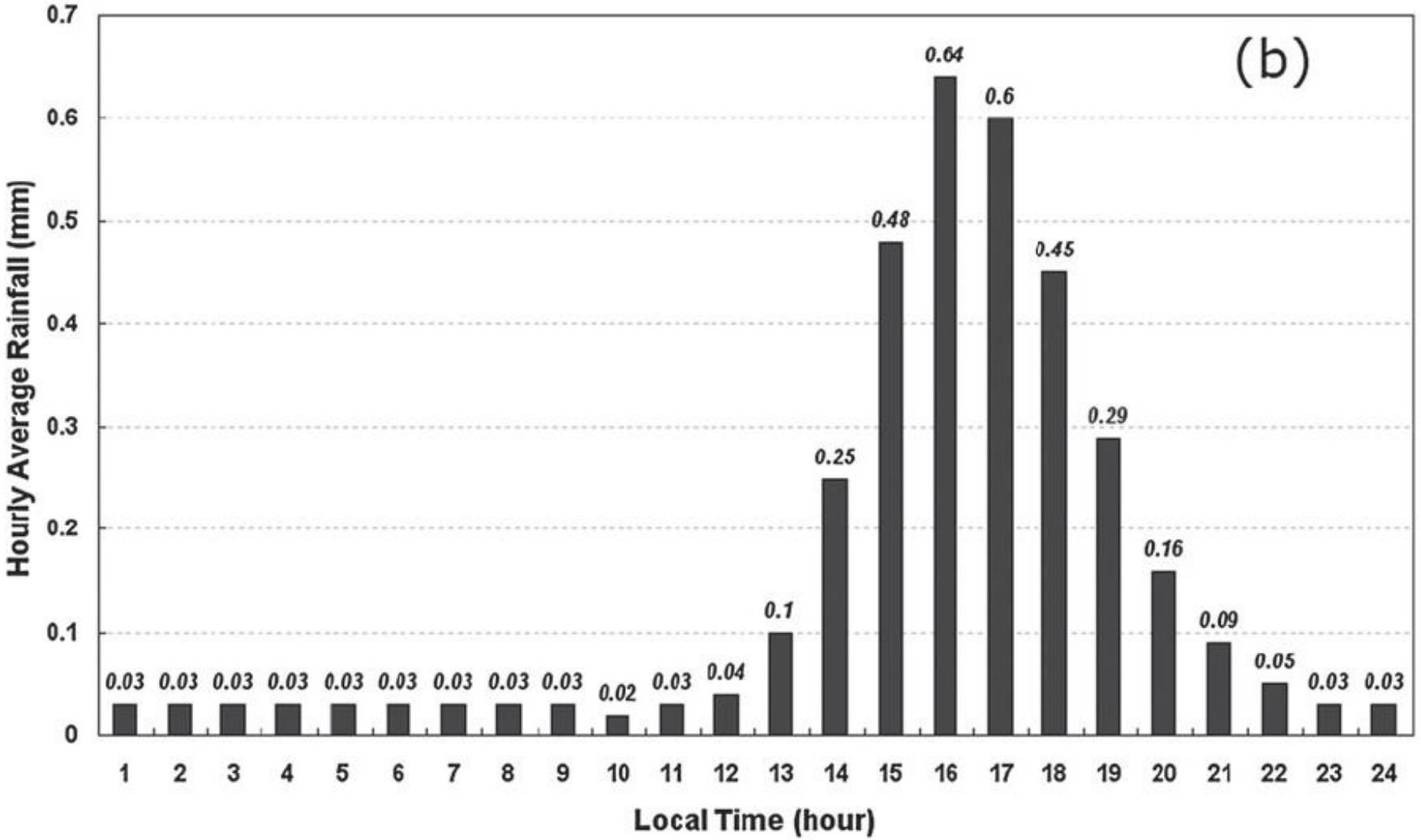

FIG. 2. (a) Distribution of rainfall amounts (mm) on undisturbed days during the warm seasons during 2005–08. Gauge stations with local precipitation maximum are labeled with the station numbers for reference. (b) Hourly average rainfall (mm) for all rain gauges. The dashed lines indicate the crest lines of two major mountain ranges (Fig. 1).

Lin et al. (2011)

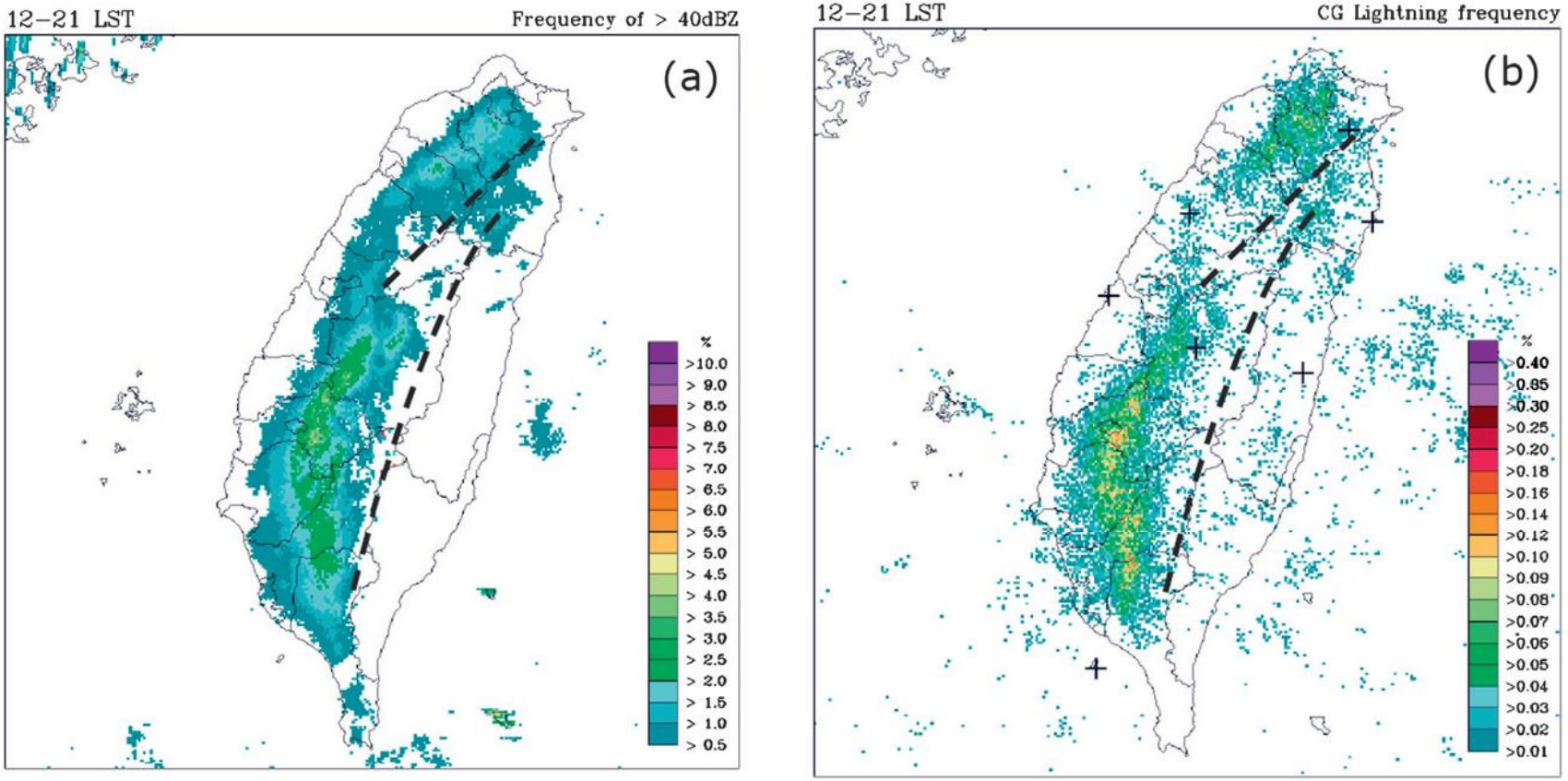

FIG. 3. Frequency of occurrence (%) of (a) reflectivity >40 dBZ and (b) CG lightning during 1200–2100 LST on undisturbed days. Seven TLDS sites are denoted by plus signs.

Lin et al. (2011)

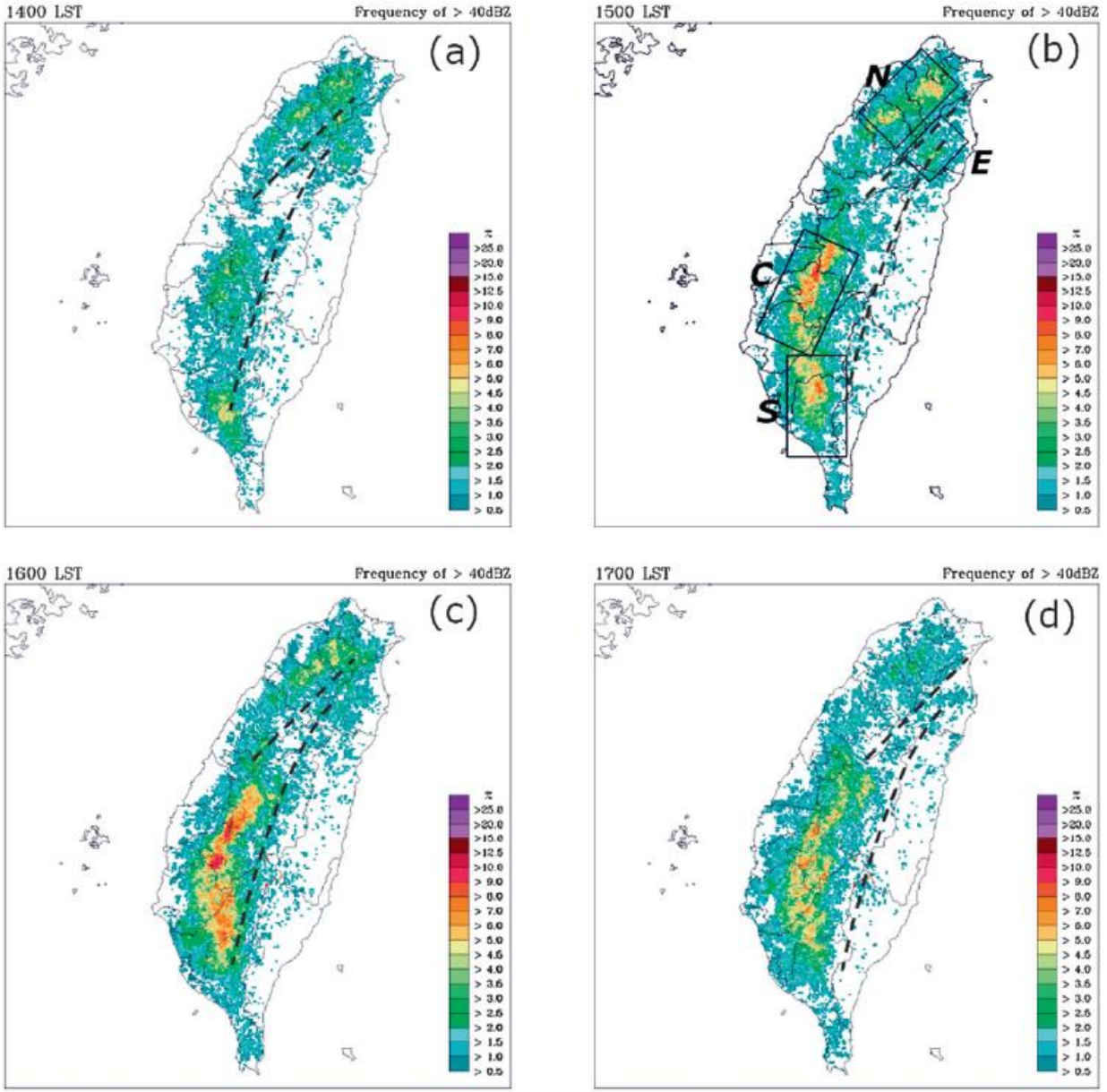

FIG. 5. Frequency of occurrence (%) for reflectivity >40 dBZ at (a) 1400, (b) 1500, (c) 1600, (d) 1700, (e) 1800, and (f) 1900 LST on undisturbed days. The four inset boxes in (b) indicate the subdomains for calculating the Hovmöller diagrams and the movement of storm cells in Figs. 6 and 7.

Lin et al. (2011)

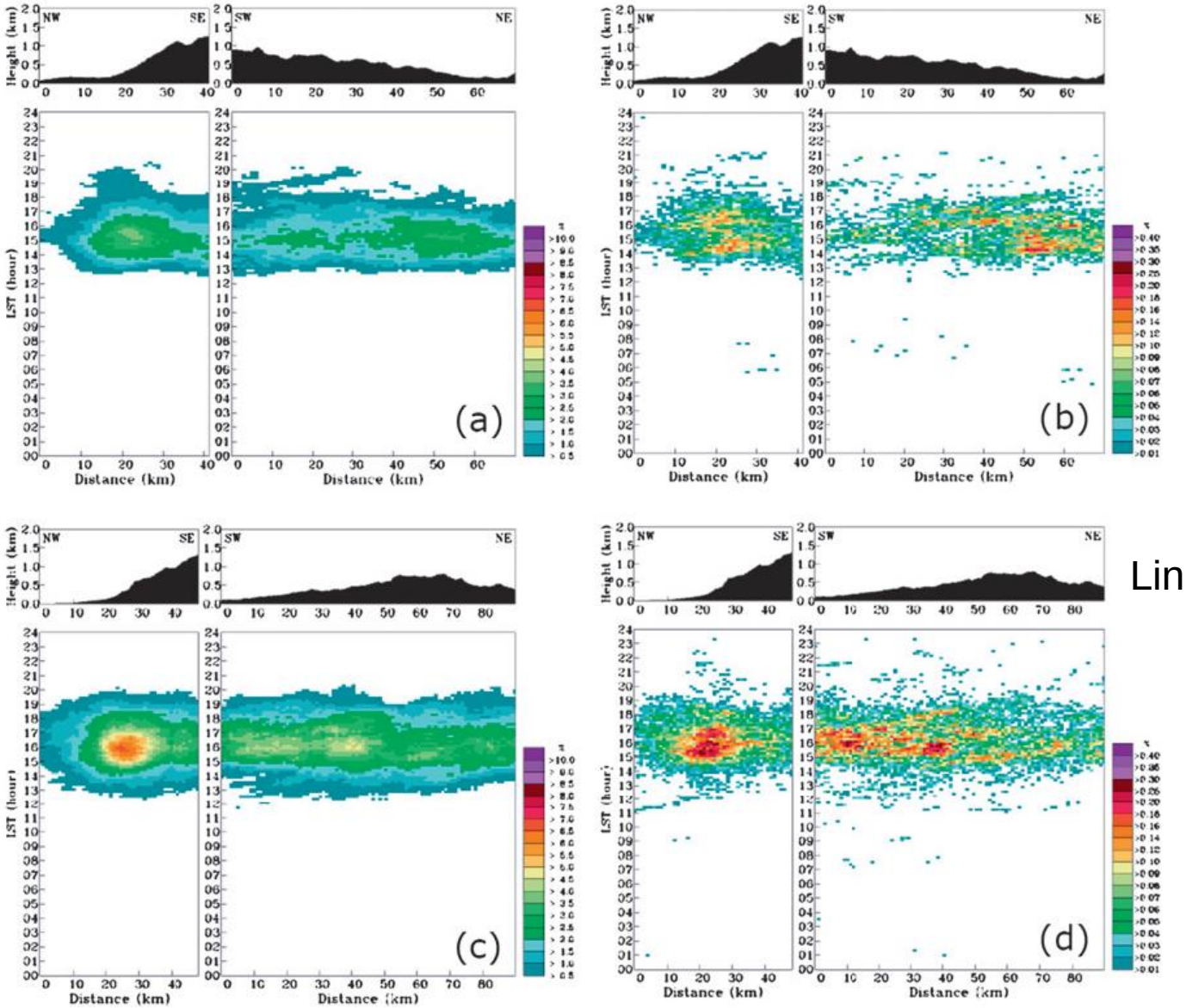

Lin et al. (2011)

FIG. 6. Hovmöller diagrams of the frequency of occurrence (%) of reflectivity >40 dBZ on undisturbed days for subdomains (a) N, (c) C, (e) S, and (g) E. (b),(d),(f), and (h) As in (a),(c),(e), and (g), but for the CG lightning. In each Hovmöller diagram, the frequency in the left (right) panel is averaged across (along) the long side of the subdomain as indicated in Fig. 5b. The average topographic profile is also indicated at the top of each panel.

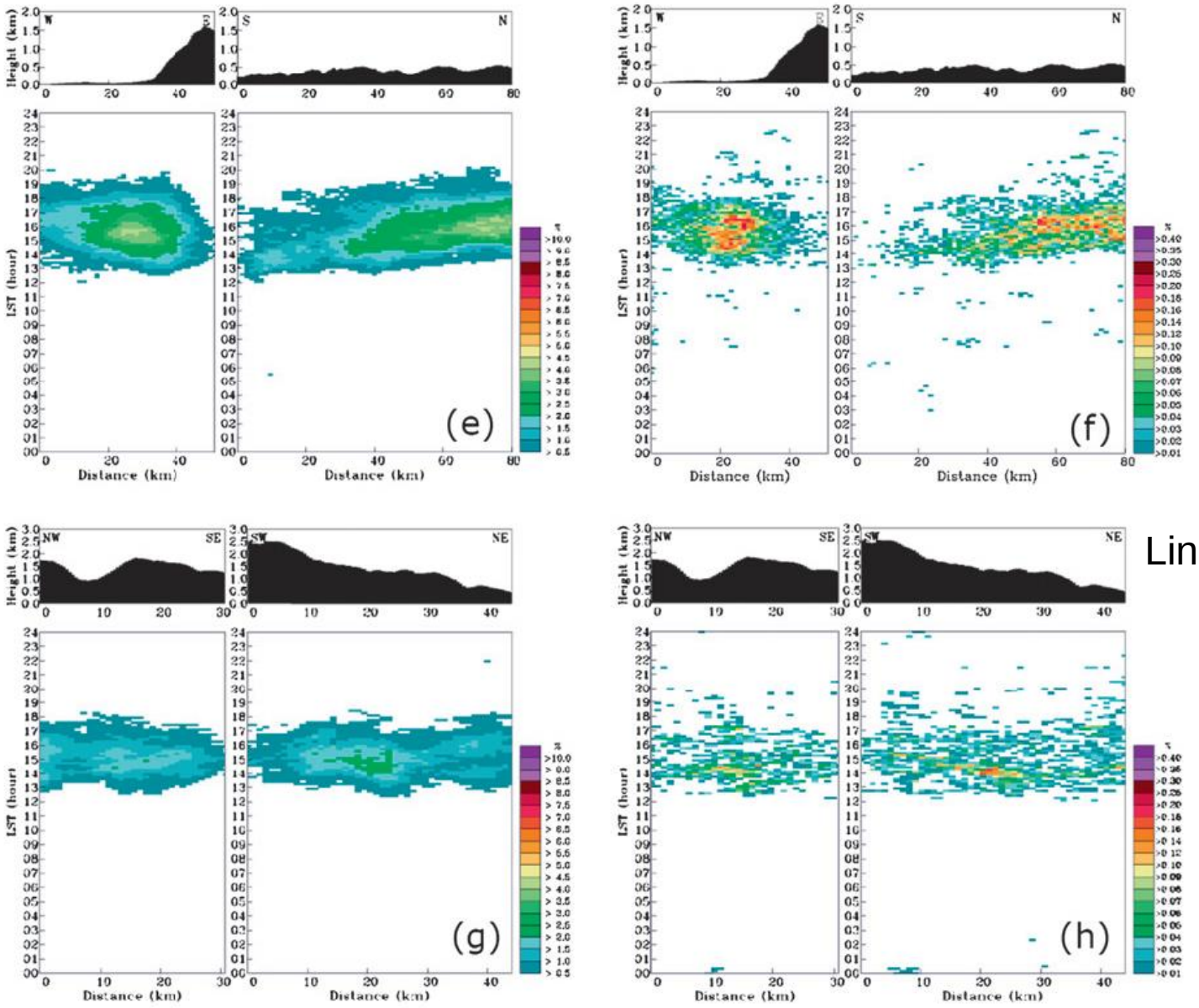

Lin et al. (2011)

FIG. 6. Hovmöller diagrams of the frequency of occurrence (%) of reflectivity >40 dBZ on undisturbed days for subdomains (a) N, (c) C, (e) S, and (g) E. (b),(d),(f), and (h) As in (a),(c),(e), and (g), but for the CG lightning. In each Hovmöller diagram, the frequency in the left (right) panel is averaged across (along) the long side of the subdomain as indicated in Fig. 5b. The average topographic profile is also indicated at the top of each panel.

TABLE 2. Total days per month with (without) afternoon thunderstorms in northern (N), central (C), southern (S) and eastern (E) Taiwan during the warm seasons (May–October) of 2005–08.

Categories	Subdomain	May	Jun	Jul	Aug	Sep	Oct	Total
TS_A (non-TS_A)	N	8 (32)	22 (29)	31 (49)	18 (39)	10 (35)	0 (4)	89 (188)
	C	8 (32)	26 (25)	53 (27)	35 (22)	23 (22)	0 (4)	145 (132)
	S	5 (35)	15 (36)	28 (52)	28 (29)	18 (27)	0 (4)	94 (183)
	E	2 (38)	12 (39)	19 (61)	12 (45)	4 (41)	0 (4)	49 (228)

Lin et al. (2011)

=> Most TS_A days occur in June, July, and August.

Note that TS_A stands for ThunderStorm in the Afternoon

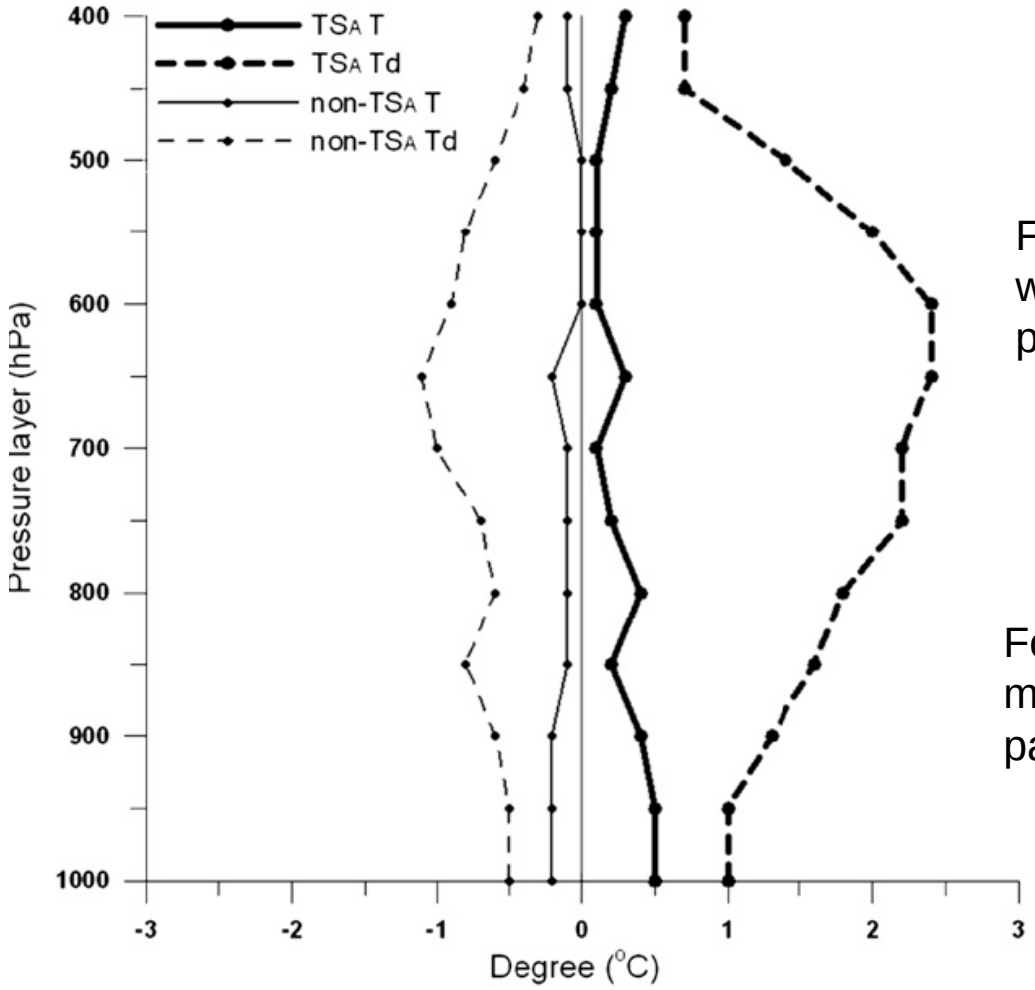

FIG. 9. Vertical profiles of mean temperature (solid line) and dewpoint temperature (dashed line) differences between the mean profiles from undisturbed days vs TS_A (heavy line) and non-TS_A (thin line) days (Table 2). The average profiles were noted at the Panchiao station (46692) in northern Taiwan taken at 0800 LST (0000 UTC).

For the TS_A days, the T profile is much warmer than that of the non-TS_A day, particularly below 850 hPa.

For the TS_A days, the Td profile is much moister than that of the non-TS_A day, particularly for 850-500 hPa.

Lin et al. (2011)

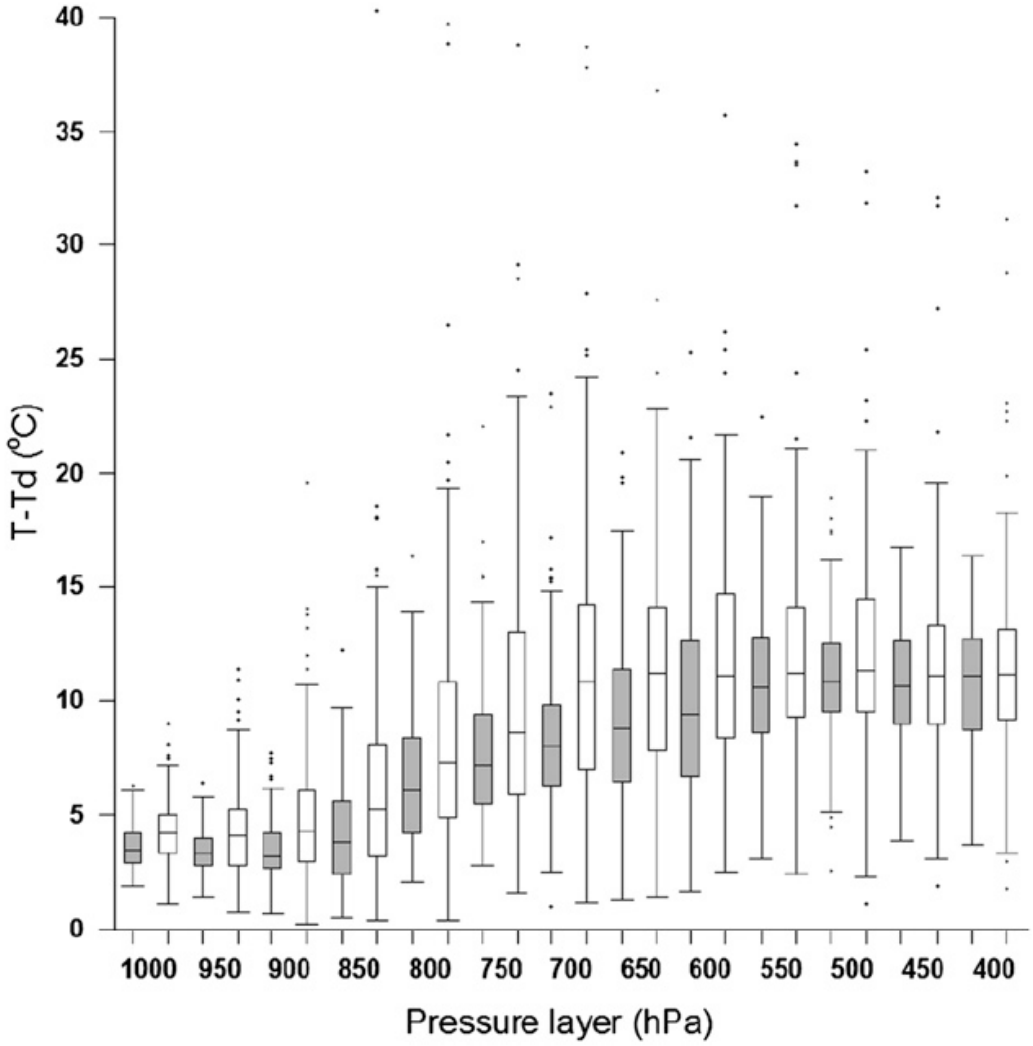

FIG. 10. Box-and-whiskers plot of T–Td from 1000 to 400 hPa for the TS_A days (gray) and non-TS_A days (white). The bottom and top of the box are the value of the first (Q1) and third (Q3) quartiles, respectively. The line in the box represents the median value. Outliers are the points that fall below Q1 − 1.5(IQR) or above Q3 + 1.5(IQR) (as the length of whiskers), where the IQR (interquartile range) is equal to the difference between Q3 and Q1.

For the TS_A days, the air is much moister than that of the non-TS_A days, particularly for 850-500 hPa.

Lin et al. (2011)

TS_A day

Non-TS_A day

0-3 km

3-6 km

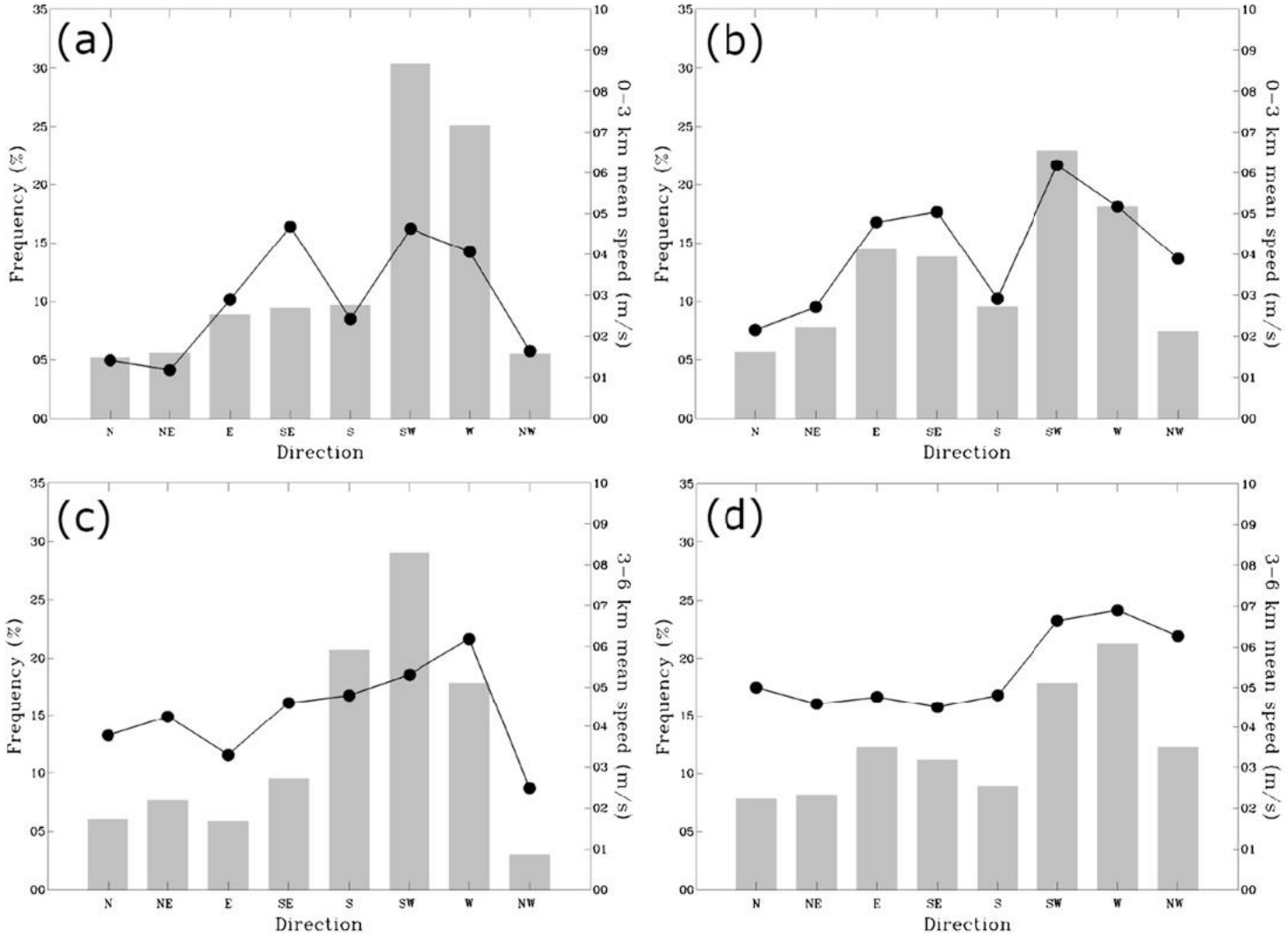

FIG. 11. Histograms of the frequencies of the observed wind directions between (a) 0–3 and (c) 3–6 km by radiosonde observations at Panchiao at 0800 LST (0000 UTC) on TS_A days. (b),(d) As in (a),(c), but for non-TS_A days. The corresponding average wind speeds are plotted with thick black lines.

Lin et al. (2011)

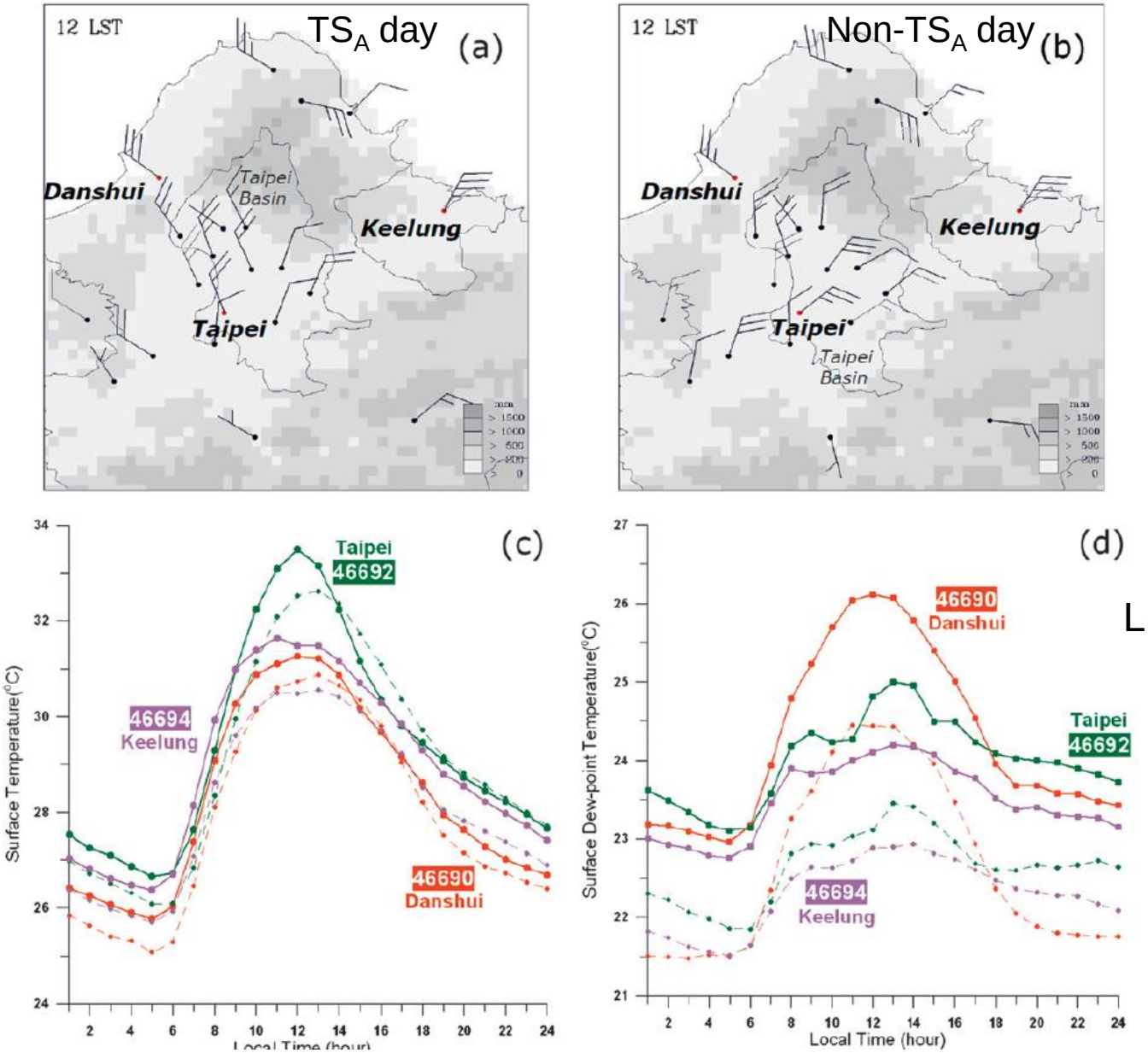

Lin et al. (2011)

FIG. 12. Hourly average surface wind at 1200 LST on (a) TS$_A$ and (b) non-TS$_A$ days in northern Taiwan. Full-wind barbs correspond to 1 m s^{-1} and half barbs correspond to 0.5 m s^{-1}. The terrain heights are also indicated with gray shading. Hourly average (c) temperature (°C) and (d) dewpoint temperature (°C) are shown for stations 46690 (Danshui), 46692 (Taipei), and 46694 (Keelung). The locations of the surface stations are indicated in Fig. 1. TS$_A$ and non-TS$_A$ days are indicated with solid and dashed lines, respectively.

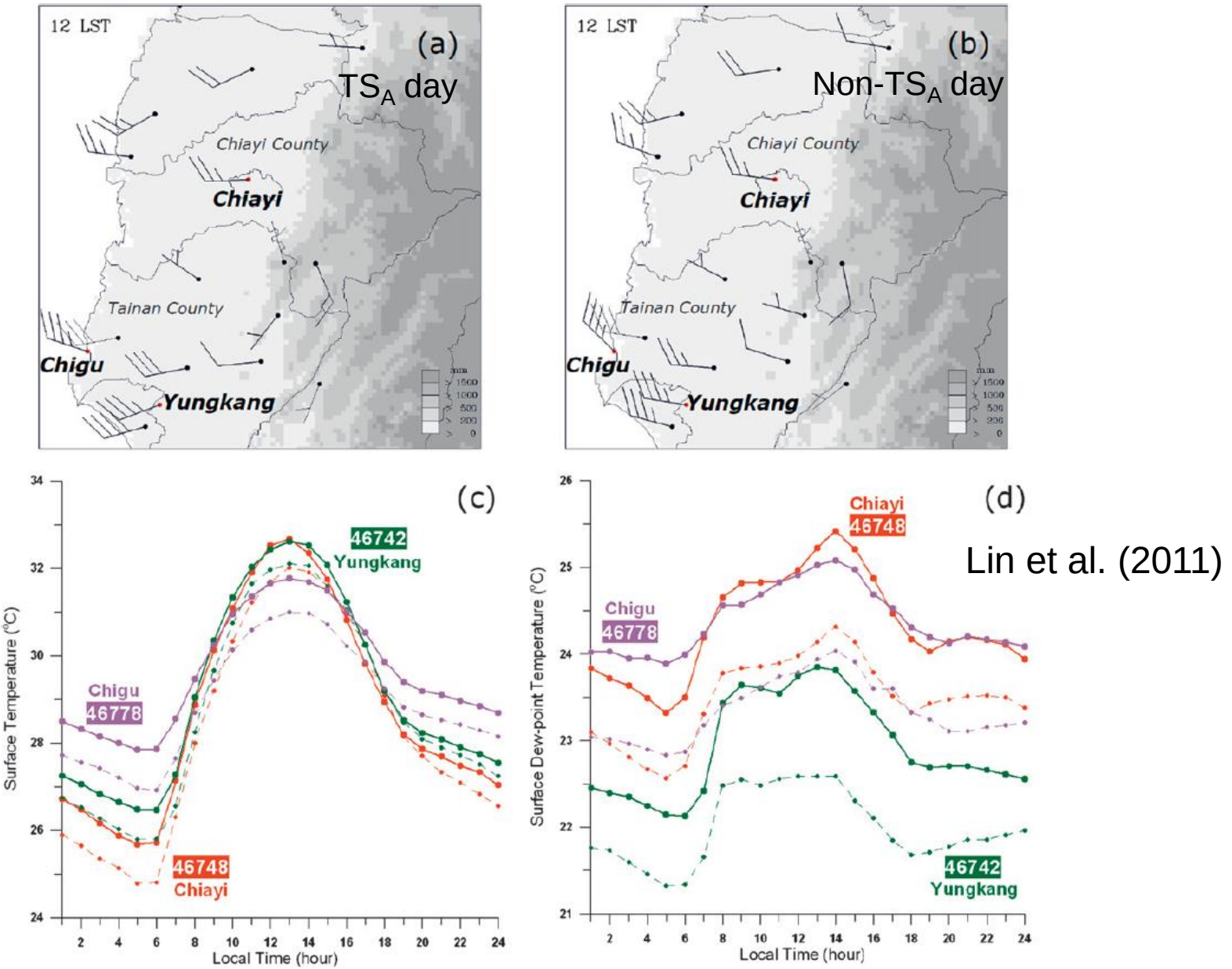

Lin et al. (2011)

FIG. 13. As in Fig. 12, but representing central Taiwan. The locations of stations 46742 (Yungkang), 46748 (Chiayi), and 46778 (Chigu) are indicated in Fig. 1.

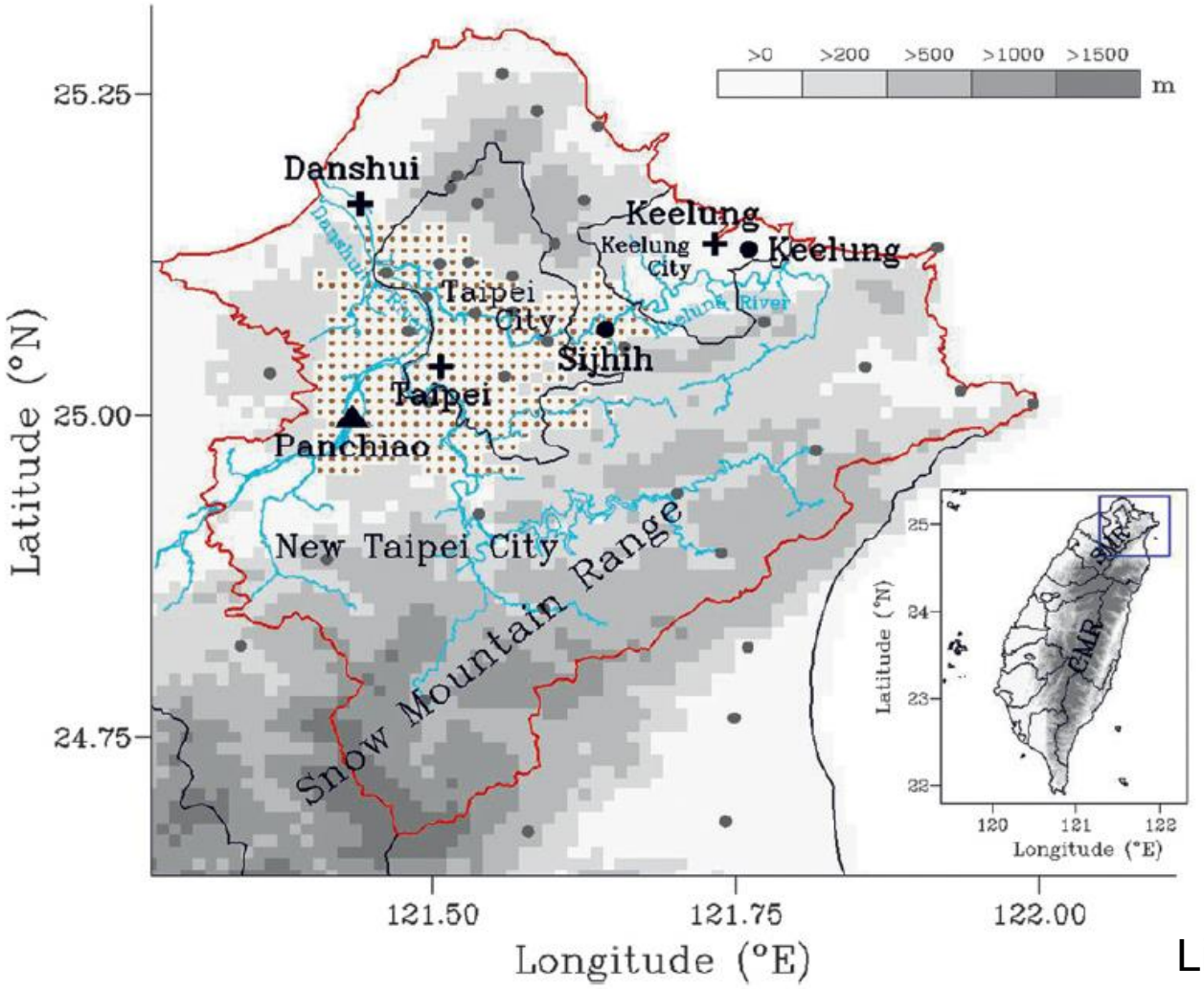

Lin et al. (2012)

FIG. 1. Distributions of observation stations in northern Taiwan. Gray shades represent terrain heights. Location of sounding site is marked with the triangle. Surface stations installed by the CWB and EPA are denoted by black plus signs and black circles, respectively. Gray circles are used as symbols for automatic meteorological stations. Surface and sounding stations used in this study are labeled with the station name for reference. The main two rivers, Danshui and Keelung (light blue lines), flowing through the Taipei Basin (brown-dotted area) are also shown. The red boundary outlines the forecast area (northern Taiwan). The blue box within the inset displays the region shown in this figure.

TABLE 1. Differences between the 148 TS_A and 127 non-TS_A days in northern Taiwan for surface stations and the composite sounding from Panchiao.

	Surface station	
	TS_A	Non-TS_A
Wind direction in the Taipei Basin	More northwestern component	More eastern component
Onset time of sea breeze from the northwest coast (LST)	0900–1000	1000–1100
Onset time of sea breeze from the northeast coast (LST)	0900–1000	0900–1000
	0800–1200 LST	
Avg temperature at the northwest coast (°C)	28.9–31.1	27.8–30.8
Avg temperature at the northeast coast (°C)	29.8–31.3	28.1–30.2
Avg temperature inland (°C)	29.2–33.5	28.0–32.1
Avg dewpoint in °C (vapor pressure in hPa) at the northwest coast	24.7–26.2 (31.1–34.0)	22.6–23.5 (27.4–28.9)
Avg dewpoint in °C (vapor pressure in hPa) at the northeast coast	23.8–24.2 (29.5–30.2)	21.9–22.2 (26.3–26.8)
Avg dewpoint in °C (vapor pressure in hPa) inland	24.0–24.7 (29.8–31.1)	22.3–22.5 (26.9–27.2)

	Composite sounding	
	TS_A	Non-TS_A
Surface temperature (°C)	27.1	26.1
Surface dewpoint depression (°C)	3.9	4.9
Layer of max difference in dewpoint depression (hPa)	850–650	850–650
CAPE (m^2 s^2)	584	0
CIN (m^2 s^2)	79	254
LCL (hPa)	951	938
Common wind direction and avg wind speed (m s^{-1}) between 0 and 3 km	Southwestern/3.4	Eastern/5.0
Common wind direction and avg wind speed (m s^{-1}) between 3 and 6 km	Southwestern/5.0	Western/6.3

Lin et al. (2012)

TS_A day

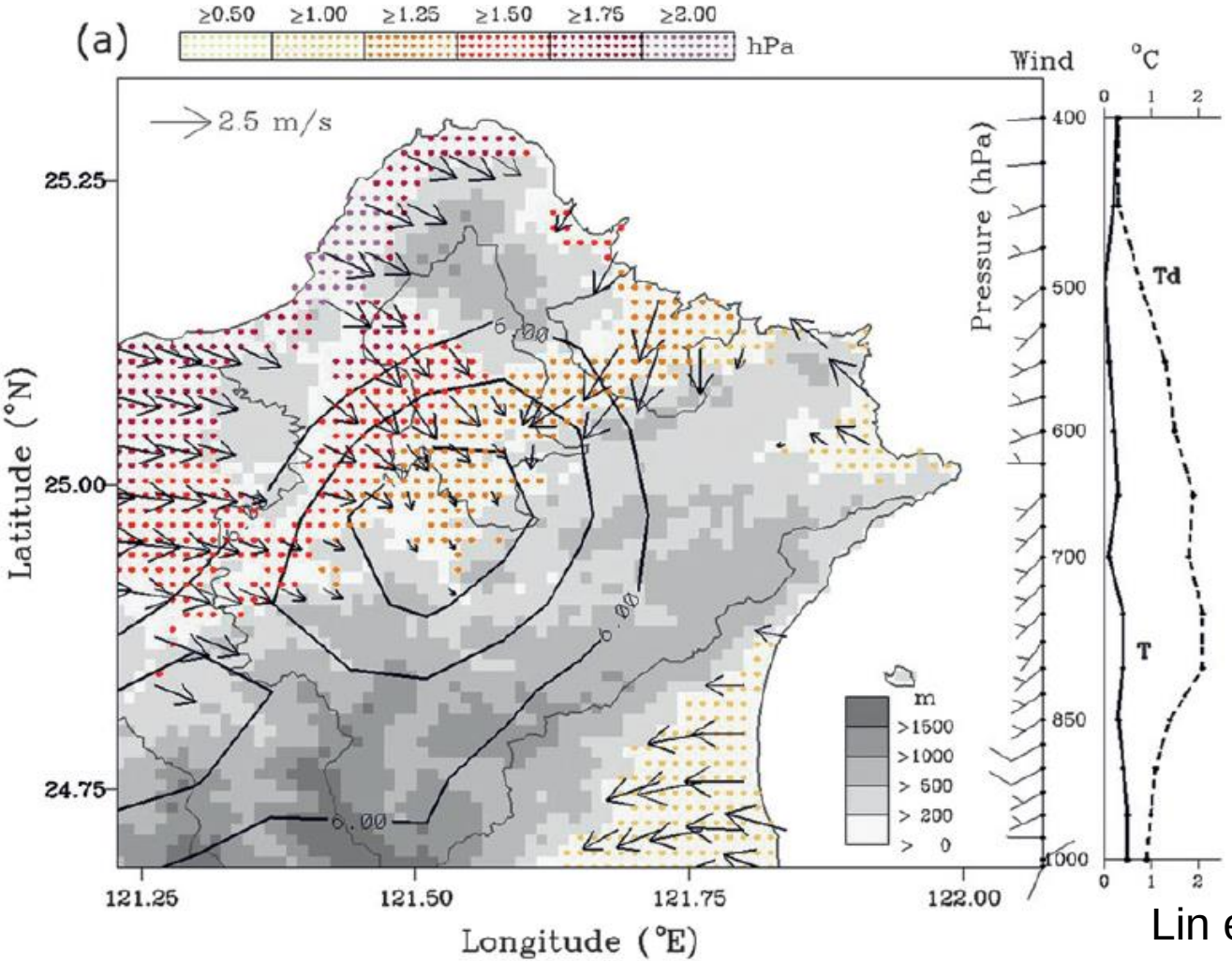

Lin et al. (2012)

FIG. 2. (a) Schematic illustration summarizing the favorable conditions during the TS_A mornings for the afternoon convective activity in northern Taiwan. Gray shades represent terrain heights. Contours show the frequency of occurrence (%) for reflectivity ≥ 40 dBZ between 1200 and 2100 LST on the TS_A days; contours start at 6% with an interval of 2%. Differences in water vapor pressures during the morning between the average from the 148 TS_A days and all undisturbed days (colored dots; see scale at top of figure) are overlaid with wind vectors (scale at top left) from surface stations and automatic meteorological stations. Vertical profiles of average temperature (solid line) and dewpoint temperature (dashed line) along the right side of the diagram are based on differences between the average profiles from all undisturbed days vs the 148 TS_A days from Panchiao soundings launched at 0800 LST. A vertical profile of the wind is also plotted with the same ordinate axis. Full wind barbs correspond to 5 m s^{-1} and half barbs correspond to 2.5 m s^{-1}. (b) As in (a), but for the non-TS_A days.

Non-TS_A day

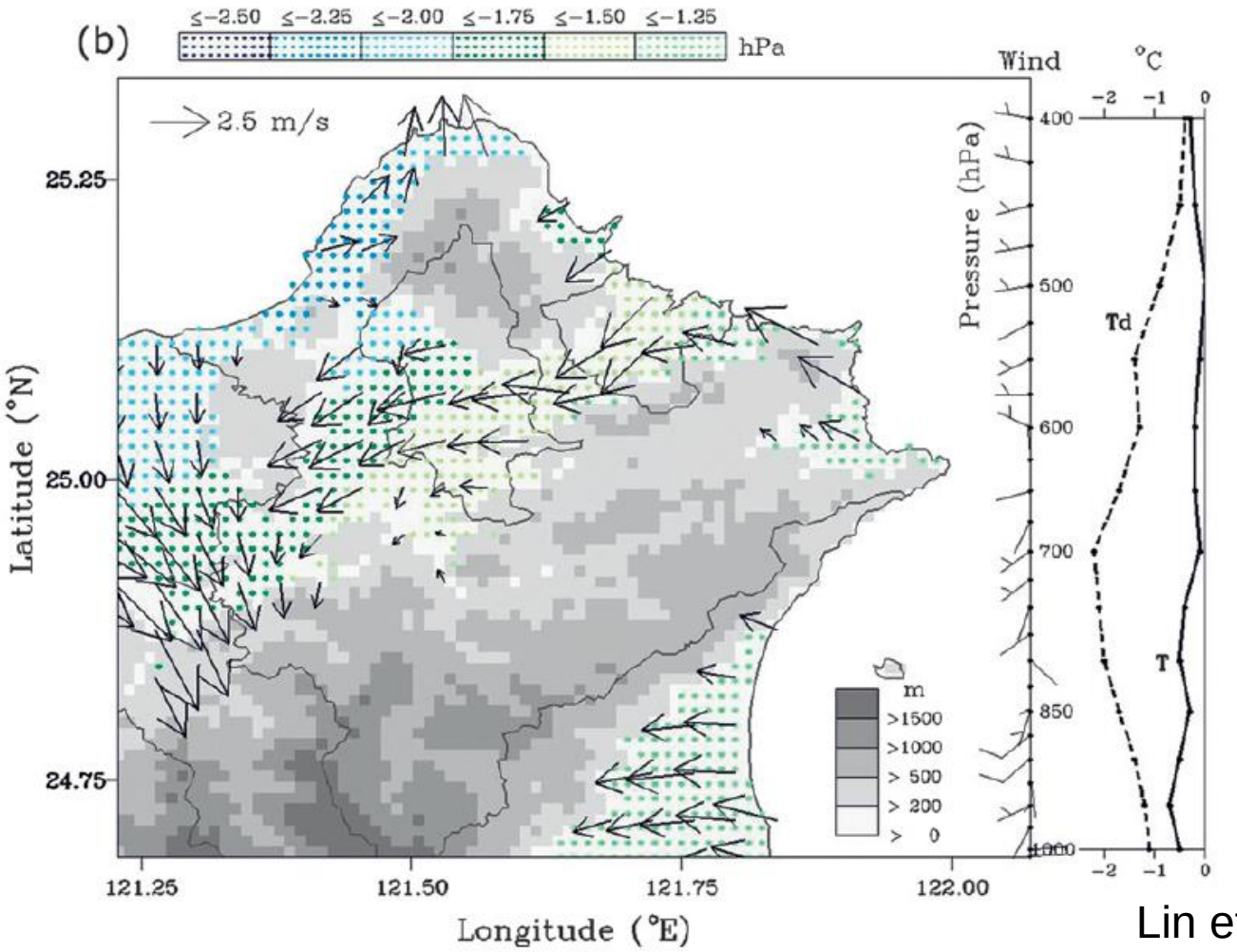

Lin et al. (2012)

FIG. 2. (a) Schematic illustration summarizing the favorable conditions during the TS_A mornings for the afternoon convective activity in northern Taiwan. Gray shades represent terrain heights. Contours show the frequency of occurrence (%) for reflectivity ≥ 40 dBZ between 1200 and 2100 LST on the TS_A days; contours start at 6% with an interval of 2%. Differences in water vapor pressures during the morning between the average from the 148 TS_A days and all undisturbed days (colored dots; see scale at top of figure) are overlaid with wind vectors (scale at top left) from surface stations and automatic meteorological stations. Vertical profiles of average temperature (solid line) and dewpoint temperature (dashed line) along the right side of the diagram are based on differences between the average profiles from all undisturbed days vs the 148 TS_A days from Panchiao soundings launched at 0800 LST. A vertical profile of the wind is also plotted with the same ordinate axis. Full wind barbs correspond to 5 m s^{-1} and half barbs correspond to 2.5 m s^{-1}. (b) As in (a), but for the non-TS_A days.

TABLE 2. References for predictors used in the fuzzy logic approach.

Boundary layer	Background information
Vapor pressure	Crook (1996): Variations in temperature and moisture in the boundary layer can be used to differentiate between no convection and intense convection
Humidity	Huntrieser et al. (1997): Relative humidity is valuable for providing the guidance for forecasting the occurrence of thunderstorms
Wind direction	Fuelberg and Biggar (1994): Low-level wind direction influences the amount of moisture that is available to convective activity and its intensity
Wind speed	Tucker and Crook (2005): Weak wind speed might lead to longer exposure of air to the concentrated heating and encourage the development of thunderstorms
Synoptic environment	**Background information**
CAPE	Adams and Souza (2009): CAPE is also frequently used as a forecasting tool for gauging severe thunderstorm likelihood since it provides a rough estimate of vertical updraft magnitude
$T - T_d$	Chen et al. (2001): Moist conditions at midlevels will reduce entrainment of dry air into growing cumulus
Wind direction	Fuelberg and Biggar (1994): Strong convection was coupled with southwesterly winds
Wind speed	Carleton et al. (2008): Land surface conditions have a greater impact on deep convection on days of weaker flow than stronger flow

Lin et al. (2012)

TABLE 9. The skill scores from all predictors (CSI-1, CSI-2, CSI-3, and CSI-4) and simplified predictors (CSI-2′, CSI-3′, and CSI-4′) at 1200 LST.

No.	Predictor		CSI-1	CSI-2	CSI-3	CSI-4	No.	Predictor		CSI-2′	CSI-3′	CSI-4′
1	Danshui	VPRE	0.560				1	Danshui	VPRE			
2		HUMD	0.486									
3		WDIR	0.648				2		WDIR			
4		WDSD	0.515									
5	Keelung	VPRE	0.518				3	Keelung	VPRE			
6		HUMD	0.440	0.726						0.700		
7		WDIR	0.530				4		WDIR			
8		WDSD	0.525									
9	Taipei	VPRE	0.465				5	Taipei	VPRE			
10		HUMD	0.343									
11		WDIR	0.517				6		WDSD			
12		WDSD	0.652									
13	CAPE		0.546				7	CAPE				
14	T-Td	1000 hPa	0.489		0.748	0.760					0.744	0.757
15		925 hPa	0.391									
16		850 hPa	0.446									
17		700 hPa	0.497									
18		500 hPa	0.400				8	T-Td	850 hPa			
19	WDIR	1000 hPa	0.298				9		700 hPa			
20		925 hPa	0.520	0.702						0.651		
21		850 hPa	0.510									
22		700 hPa	0.476									
23		500 hPa	0.301				10	WDIR	850 hPa			
24	WDSD	1000 hPa	0.601				11		700 hPa			
25		925 hPa	0.520									
26		850 hPa	0.461									
27		700 hPa	0.518									
28		500 hPa	0.475									
29	PRST		0.542	0.542	0.542		12	PRST		0.542	0.542	

Lin et al. (2012)

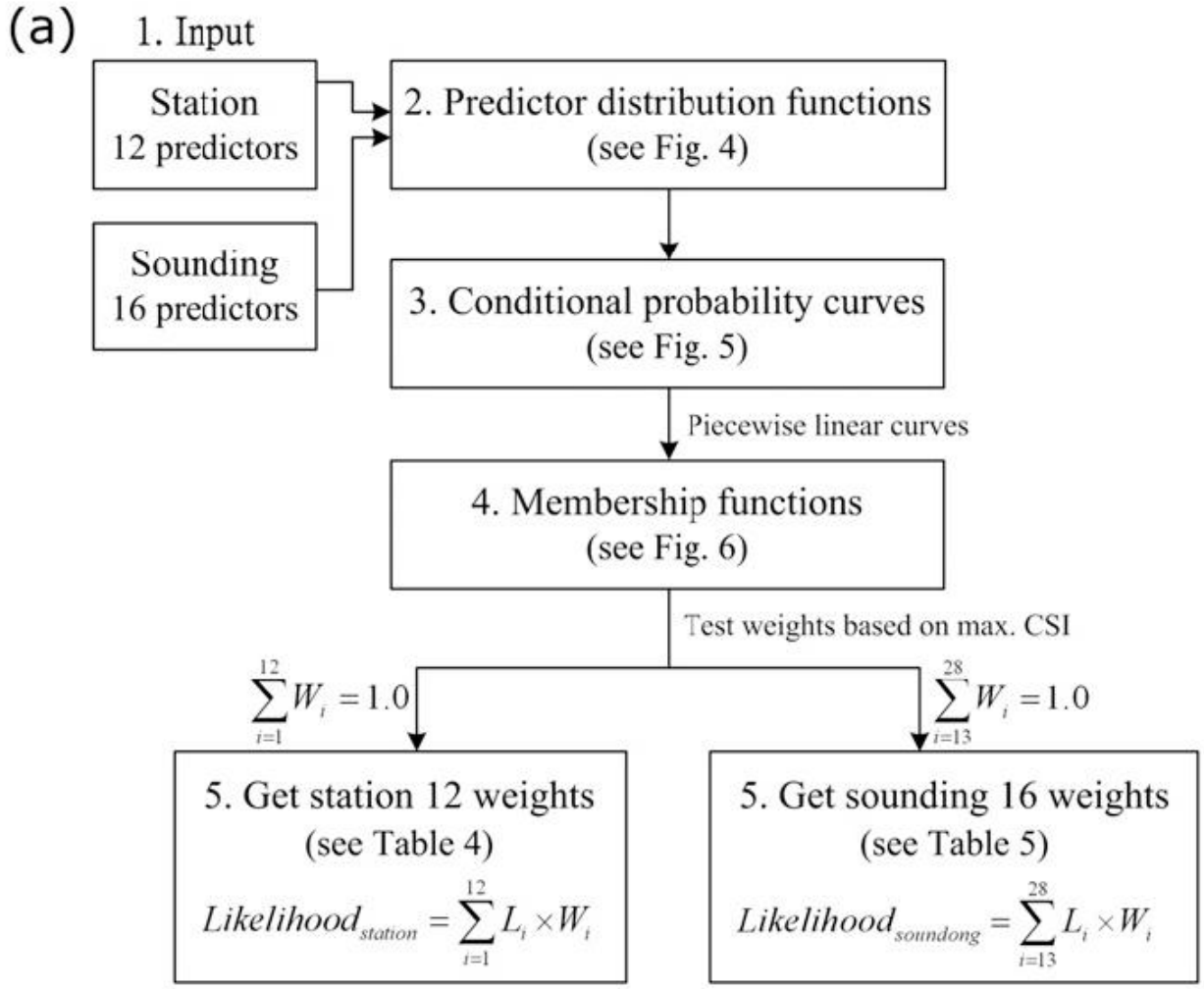

FIG. 3. Schematic of the fuzzy logic algorithm for forecasting TS_A. (a) The procedure for determining weights separately for surface station and sounding predictors. (b) The procedure for determining weights for a set of three predictors, SOUNDING (large-scale environment), STATION (local influences), and PERSISTENCE. Here, the *L* and *W* are the representatives of likelihood and weight, respectively. Each step is expatiated in the text.

Lin et al. (2012)

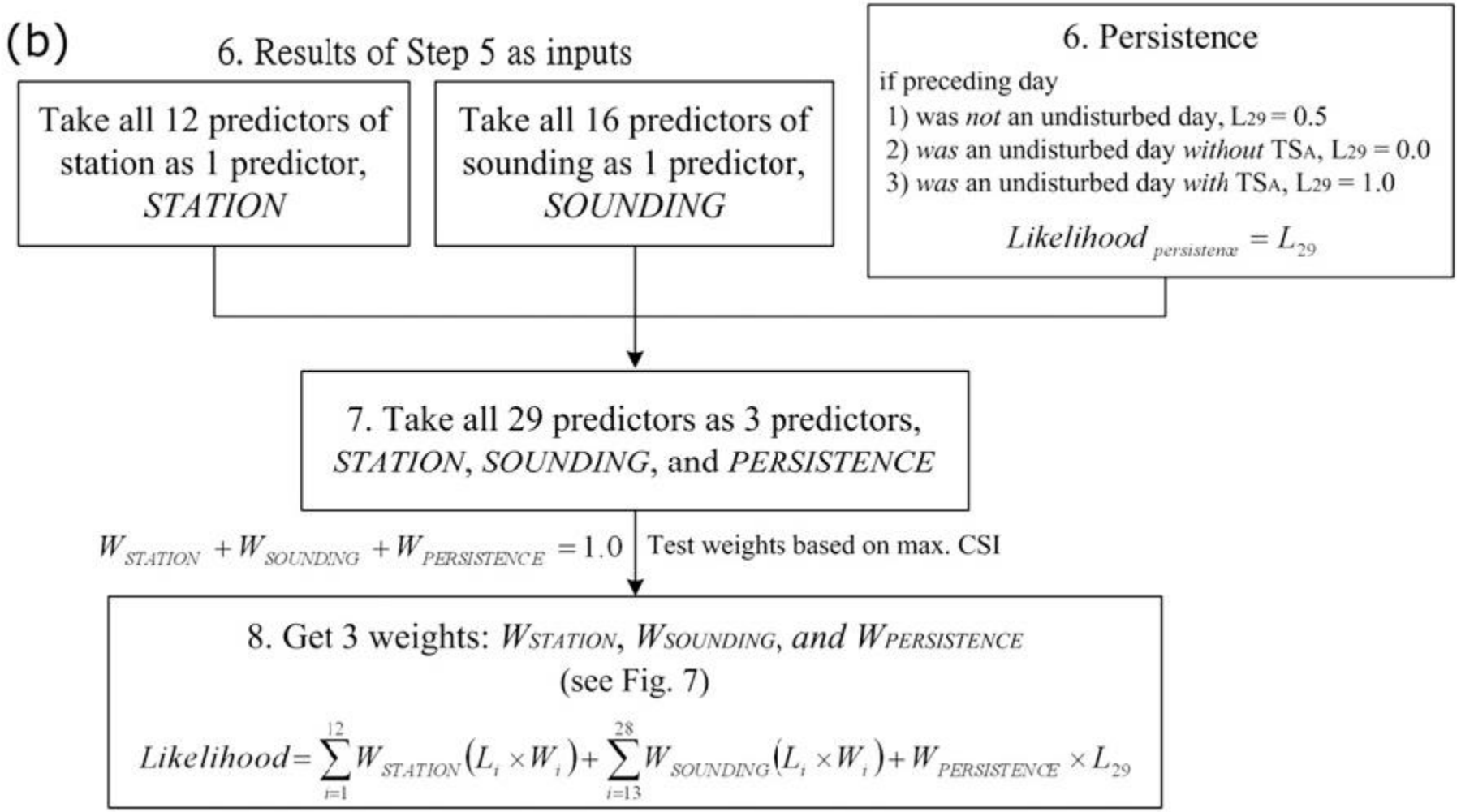

FIG. 3. Schematic of the fuzzy logic algorithm for forecasting TS_A. (a) The procedure for determining weights separately for surface station and sounding predictors. (b) The procedure for determining weights for a set of three predictors, SOUNDING (large-scale environment), STATION (local influences), and PERSISTENCE. Here, the *L* and *W* are the representatives of likelihood and weight, respectively. Each step is expatiated in the text.

Lin et al. (2012)

a. Predictor distribution functions

The frequency distributions for each feature X_k (vapor pressure, wind direction, CAPE, etc.), conditional to the day type s (TS_A and non-TS_A days) can be expressed as follow (Berenguer et al. 2006):

$$f_{k,s}(x) = p(X_k = x|\text{day type} = s) = \frac{n(X_k = x \cap \text{day type} = s)}{n(\text{day type} = s)}$$

where $f_{k,s}(x)$ is the frequency; subscript k indicates the different parameters; $n(X_k = x \cap \text{day type} = s)$ stands for the number of days, where $X_k = x$ and the day has been classified as type s; and $n(\text{day type} = s)$ is the total number of days classified as day type s.

Lin et al. (2012)

頻率分布函數為對任一個預報因子 k（如水氣壓、風向或 CAPE…等），當其數值 $X_k = x$ 時，發生分類 s (TS_A 或 non-TS_A day)的頻率 $f_{k,s}(x)$，可表示為(Berenguer et al. 2006)：

$$f_{k,s}(x) = \frac{n(X_k = x \cap day\ \ type = s)}{n(day\ \ type = s)}$$

其中，$n(day\ type = s)$為 TS_A day 或 non-TS_A day 的天數。

林等 (2012；大氣科學)

Lin et al. (2012)

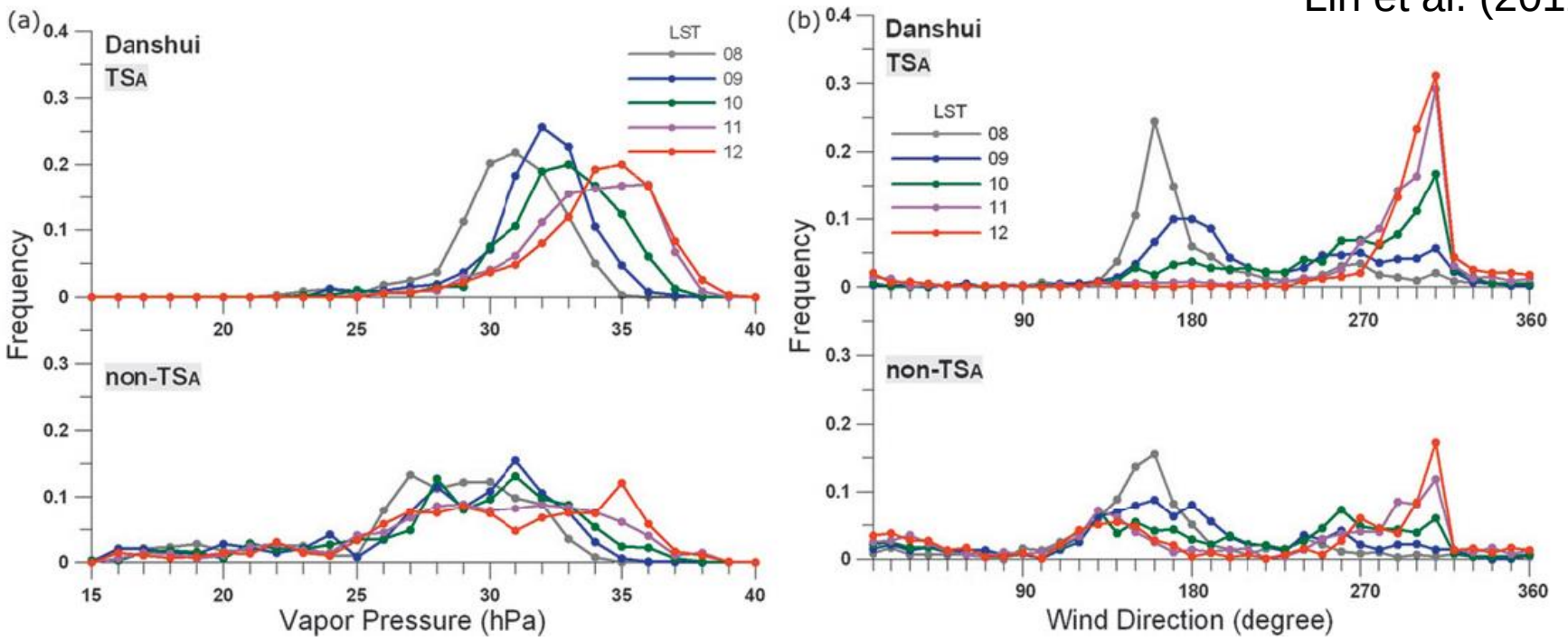

FIG. 4. Predictor distribution functions corresponding to the (top) TS_A and (bottom) non-TS_A days, derived from the surface station and sounding observations.

TS_A day

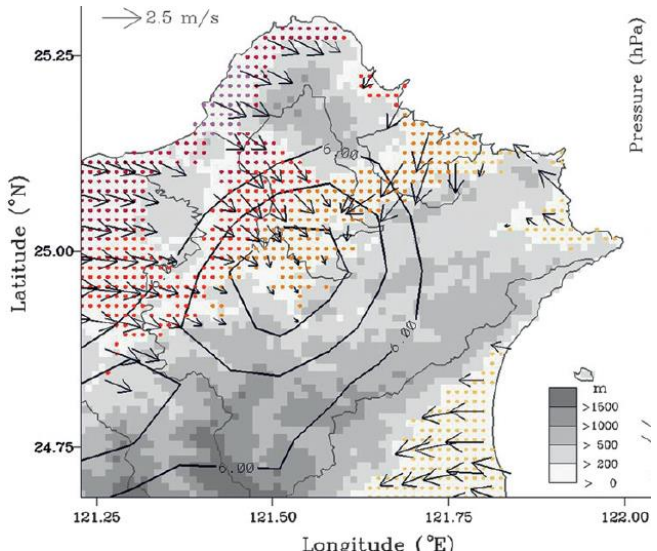

Non-TS_A day

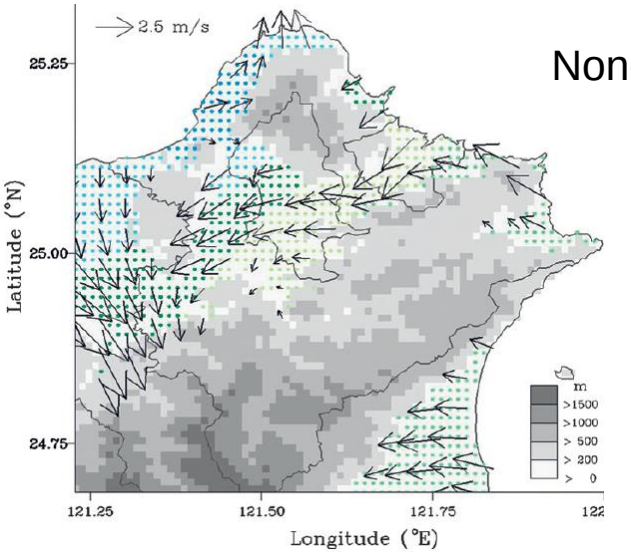

Lin et al. (2012)

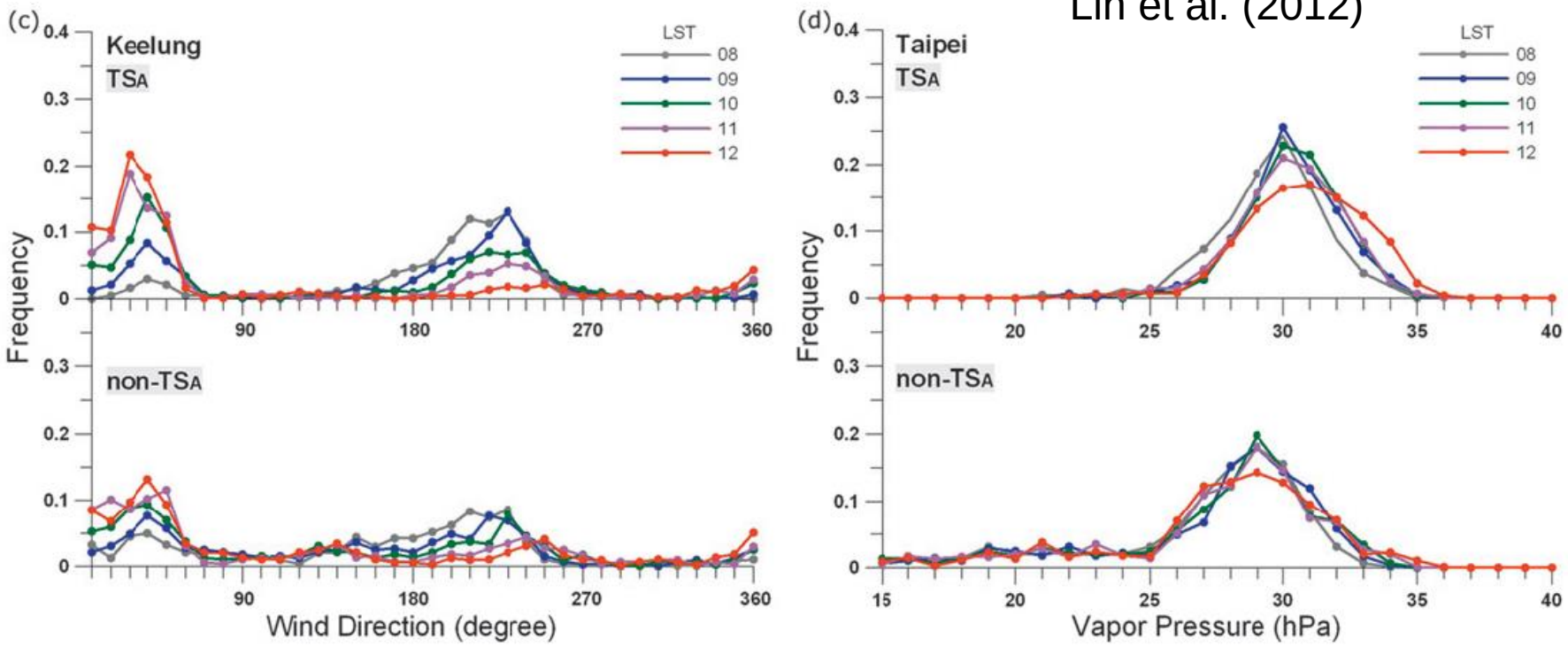

FIG. 4. Predictor distribution functions corresponding to the (top) TS_A and (bottom) non-TS_A days, derived from the surface station and sounding observations.

TS_A day

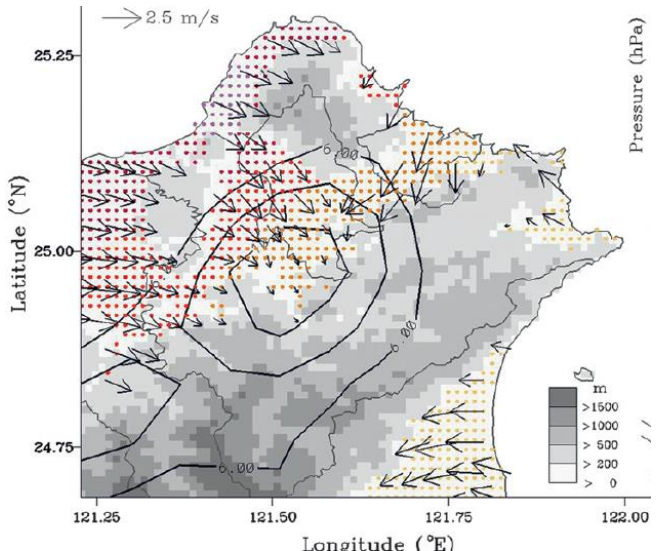

Non-TS_A day

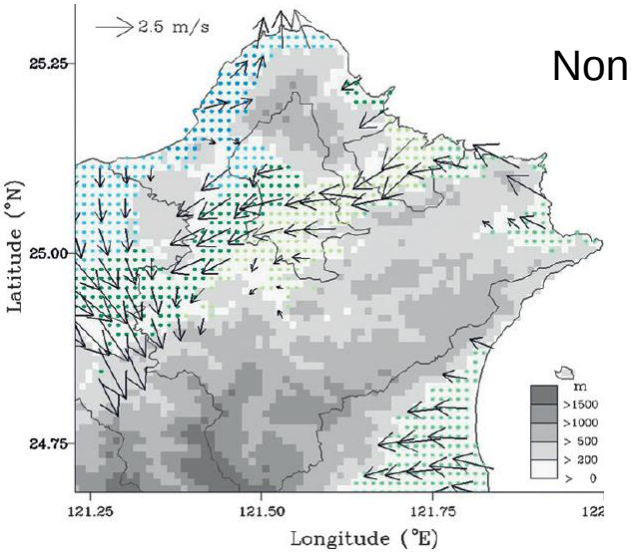

Lin et al. (2012)

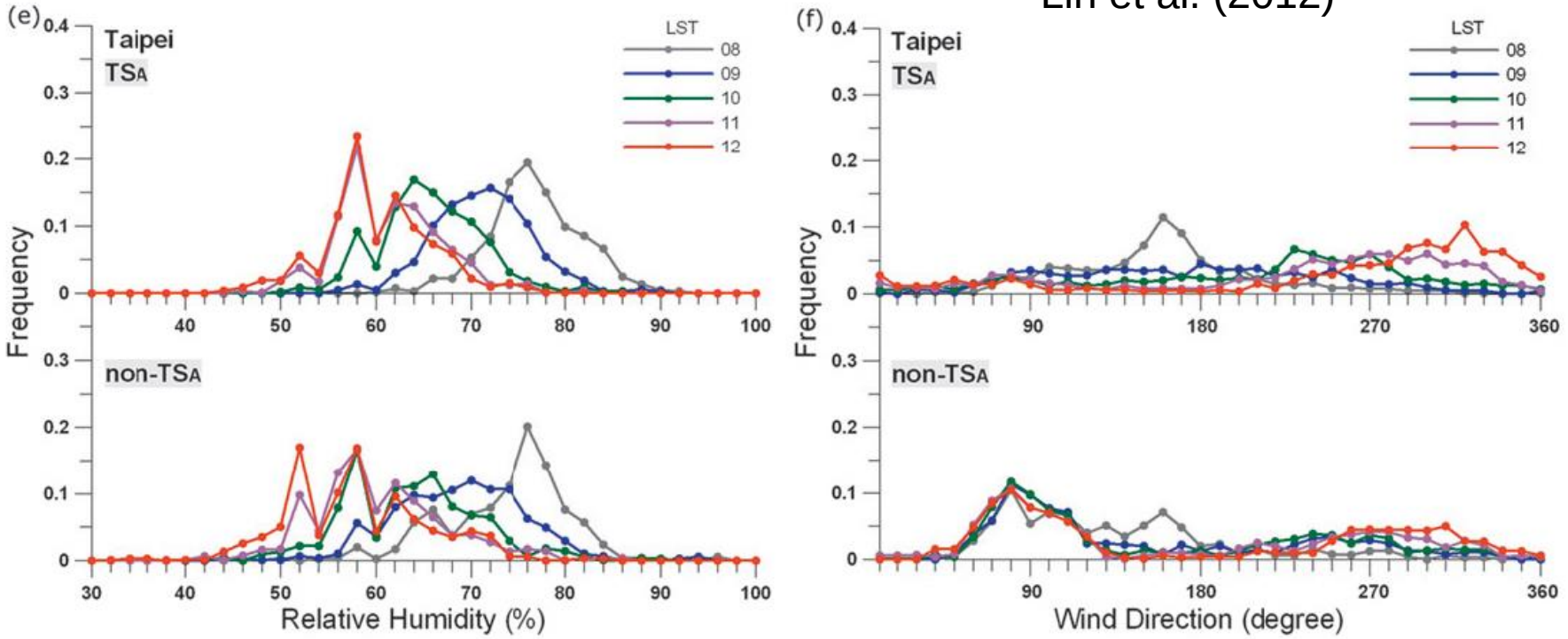

FIG. 4. Predictor distribution functions corresponding to the (top) TS_A and (bottom) non-TS_A days, derived from the surface station and sounding observations.

TS_A day

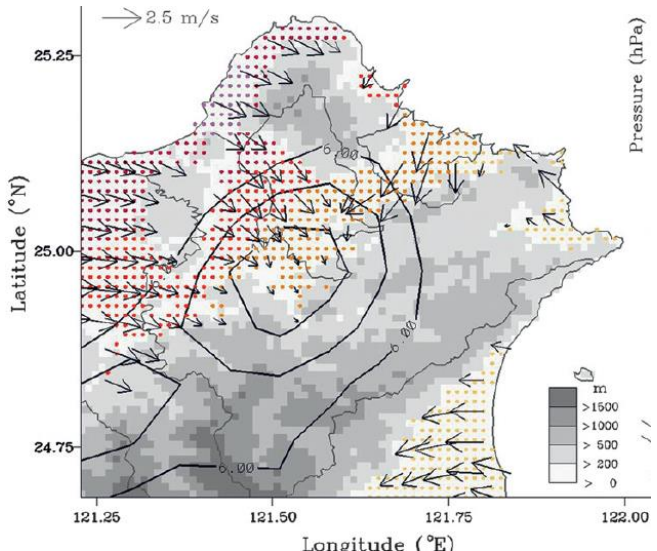

Non-TS_A day

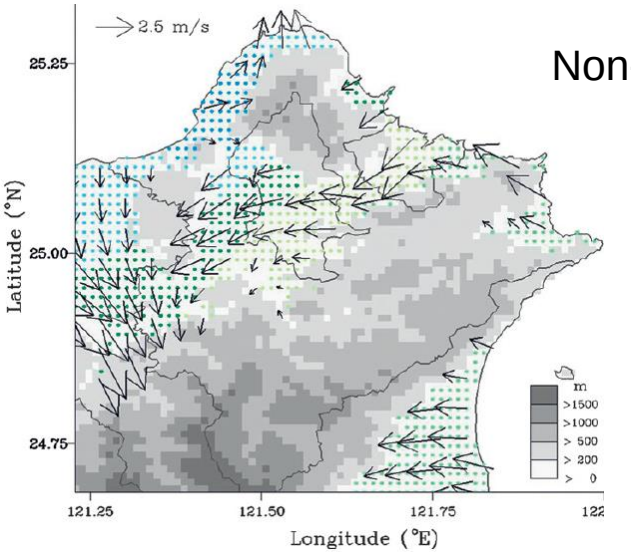

Lin et al. (2012)

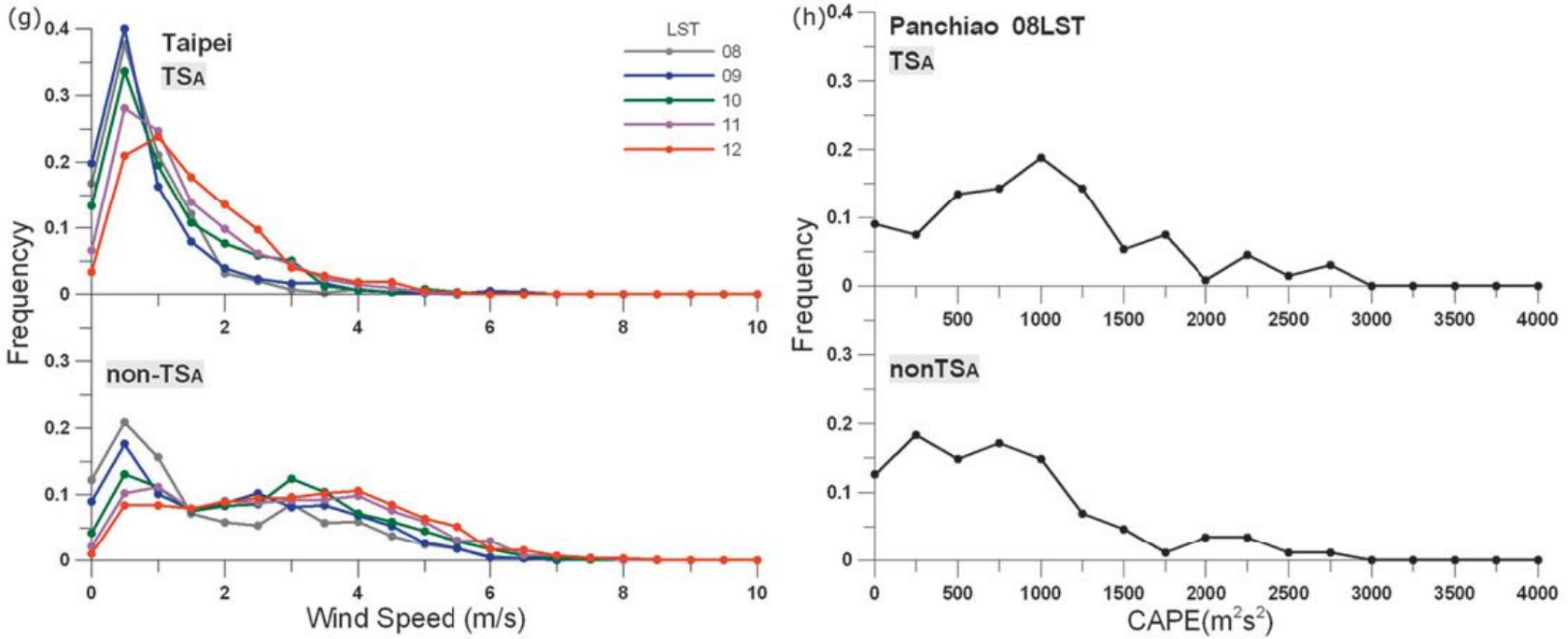

FIG. 4. Predictor distribution functions corresponding to the (top) TS_A and (bottom) non-TS_A days, derived from the surface station and sounding observations.

TS_A day

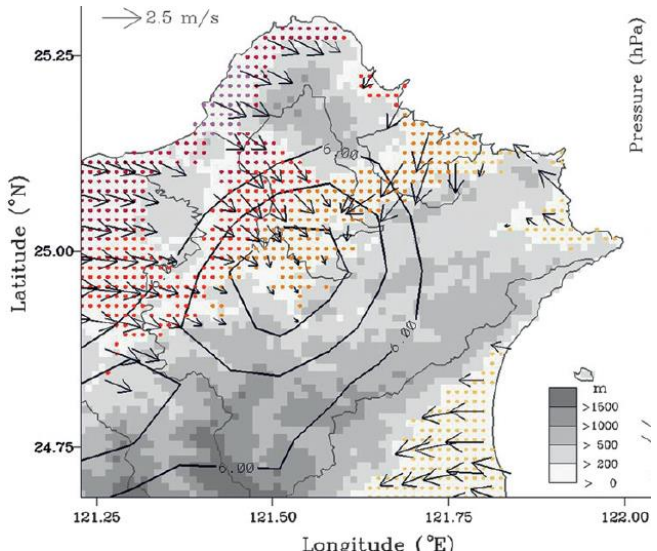

Non-TS_A day

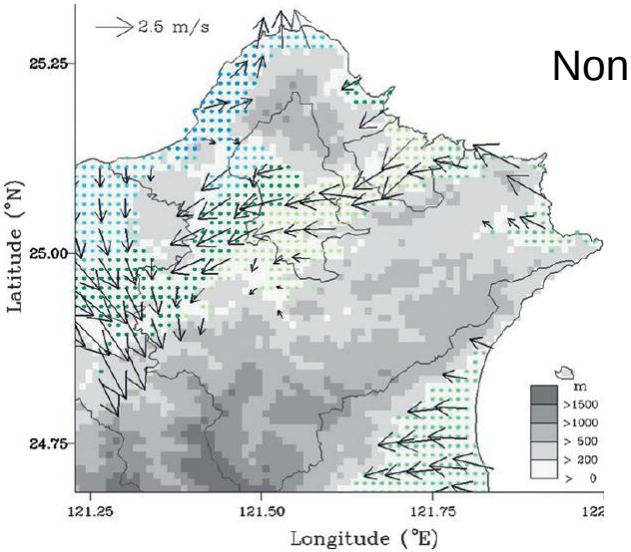

Lin et al. (2012)

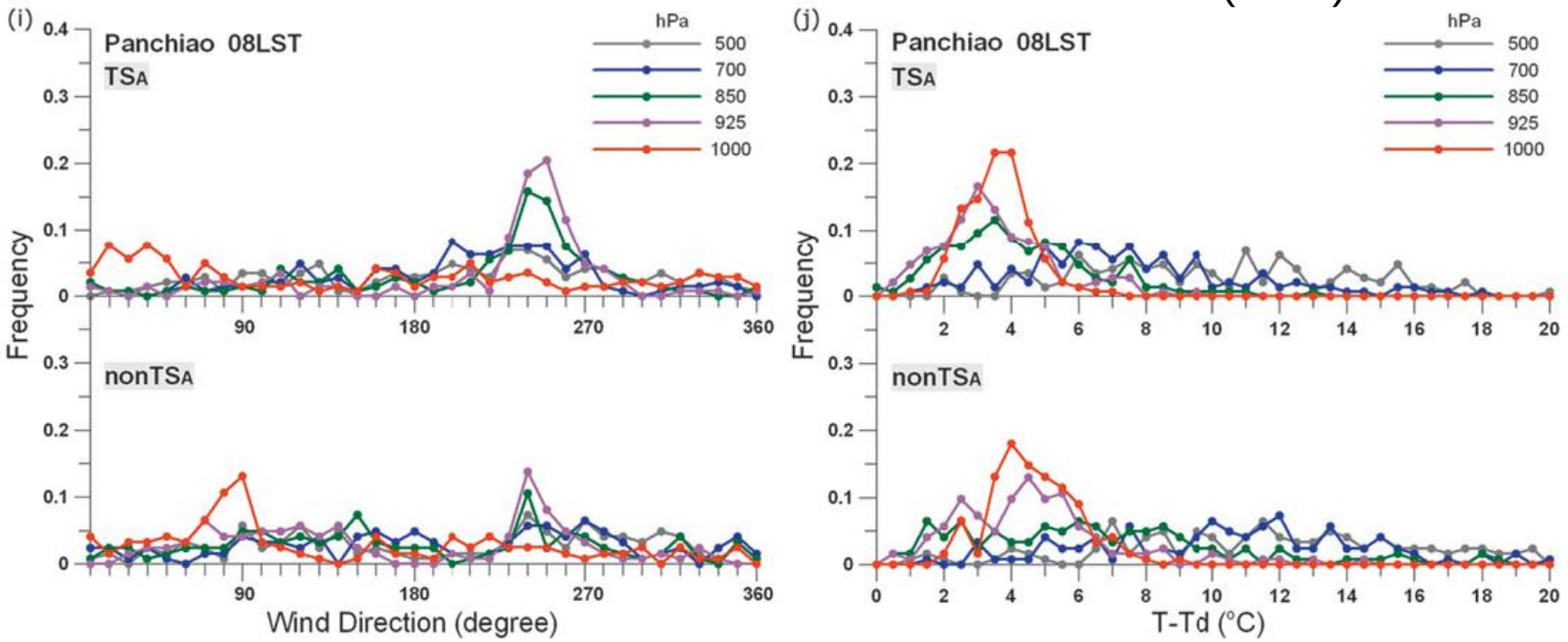

FIG. 4. Predictor distribution functions corresponding to the (top) TS_A and (bottom) non-TS_A days, derived from the surface station and sounding observations.

TS_A day

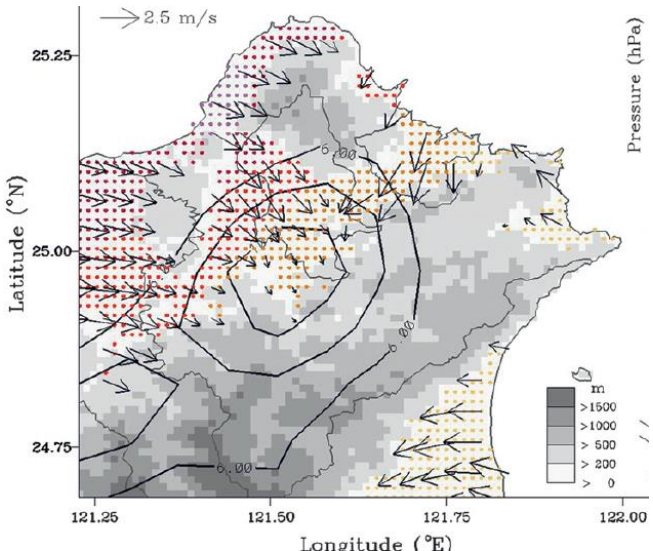

Non-TS_A day

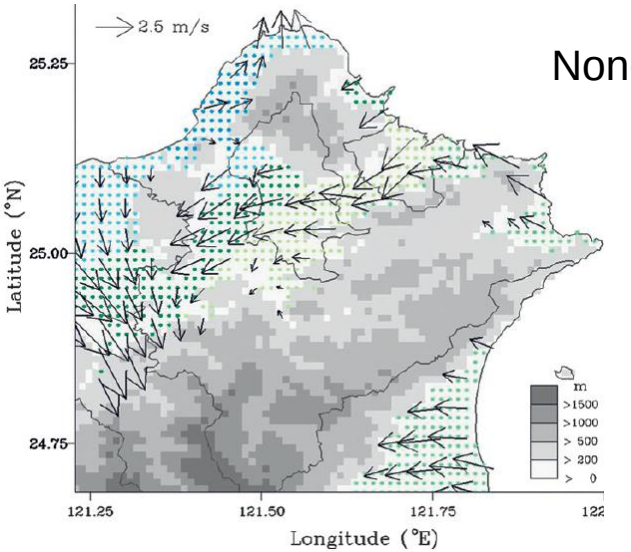

b. Conditional probability curves

After the normalized frequency distributions for each feature X_k, the conditional probability curve of a day is affected by a certain day type s when $X_k = x$; the expression is (Berenguer et al. 2006)

$$p_{k,s}(x) = p(\text{day type} = s | X_k = x) = \frac{n(X_k = x \cap \text{day type} = s)}{n(X_k = x)},$$

where $p_{k,s}(x)$ is the probability and $n(X_k = x)$ is the total number of day type s when $X_k = x$. The conditional probability curves of preconvective features and the variations can be calculated with different values of x. In this study, $p_{k,s}(x)$ indicates the conditional probability curve for the TS_A days. On the contrary, $1–p_{k,s}(x)$ exhibits the conditional probability curve for the non-TS_A days.

Lin et al. (2012)

條件機率函數為針對任一個預報因子 k，當其數值 $X_k = x$ 時，計算發生 TS_A 之機率 $p_{k,s}(x)$，可如下表示(Berenguer et al. 2006)：

$$p_{k,s}(x) = \frac{n(X_k = x \cap day \quad type = s)}{n(X_k = x)}$$

其中，$n(X_k = x)$為 X_k=x 的總天數，因此 $n(X_k = x)$在不同的預報因子及不同數值，皆非固定值。另外，因為在本研究中條件機率函數為針對 TS_A days，因此，$1 – p_{k,s}(x)$則為 non-TS_A days 的條件機率值。

林等 (2012；大氣科學)

Lin et al. (2012)

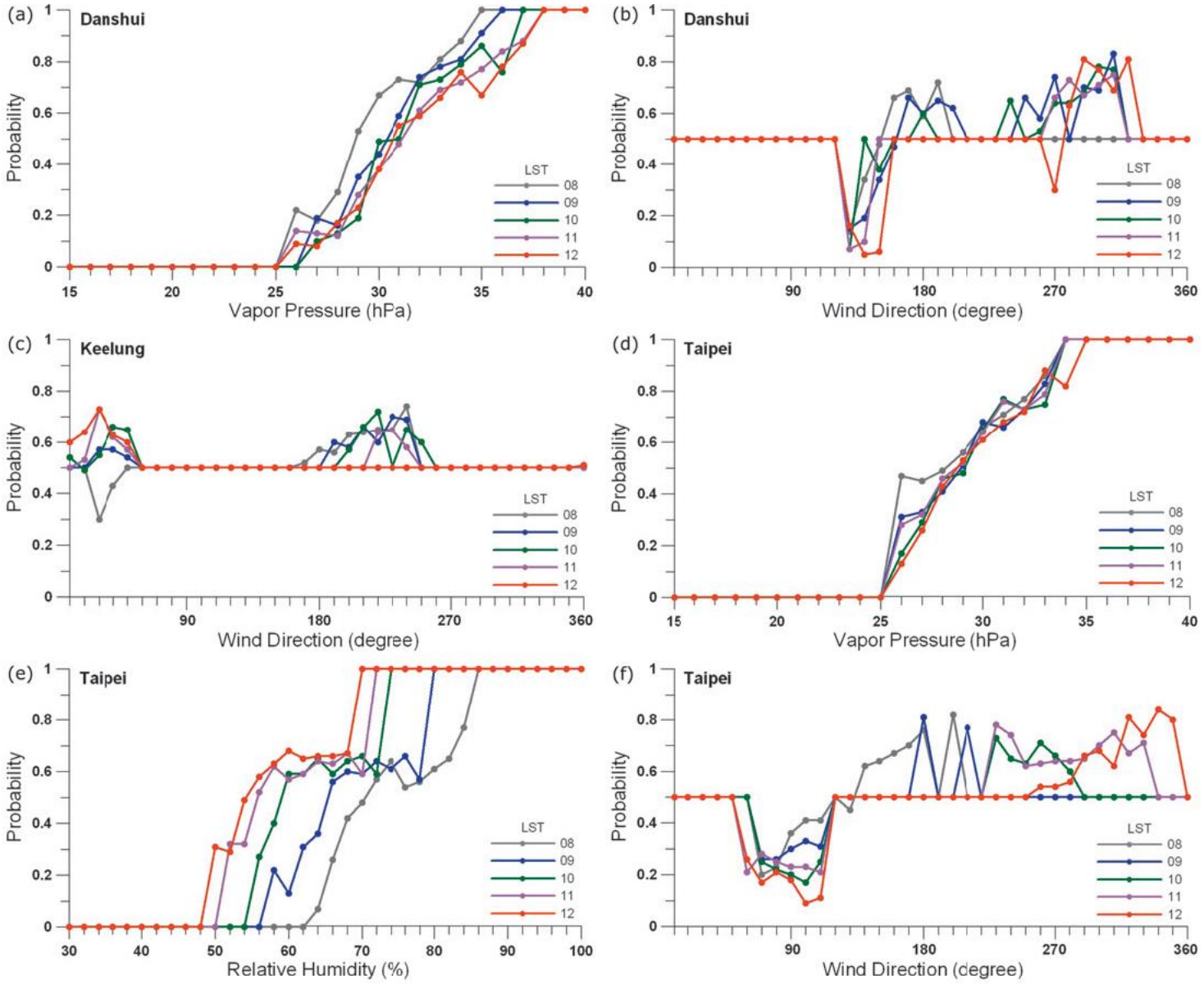

FIG. 5. Conditional probability curves corresponding to the TS_A days derived from the predictor distribution functions in Fig. 4.

Lin et al. (2012)

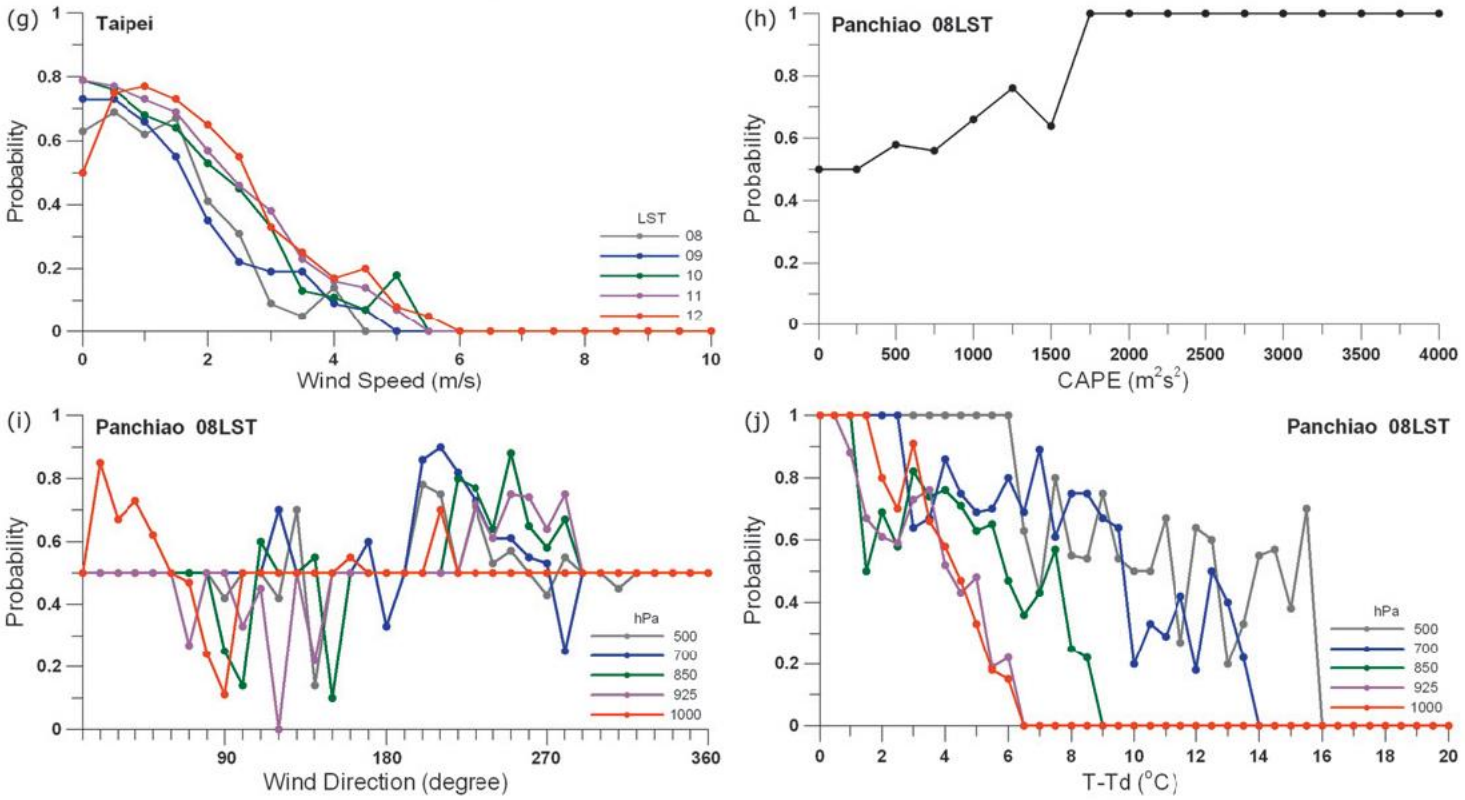

FIG. 5. Conditional probability curves corresponding to the TS_A days derived from the predictor distribution functions in Fig. 4.

TABLE 3. Favorable (probability > 0.5) hourly preconvective conditions and predictors for TS_A occurrence using conditional probability curves.

Station	Hour (LST)	0800	0900	1000	1100	1200
Danshui	VPRE (hPa)	29	30.5	31	31.5	31
	HUMD (%)	74	70.5	69	67.5	67
	WDIR (°)	160–190	250–310	240–310	270–310	280–320
	WDSD (m s^{-1})	<1.5	<2.0	<2.0	<3.5	<4.5
Keelung	VPRE (hPa)	28.5	28	28.5	28.5	28.5
	HUMD (%)	68	61	61.5	59	62
	WDIR (°)	170–240	30–50	10–50	20–50	0–50
	WDSD (m s^{-1})	<3.0	<2.5	<3.5	<4.0	<4.5
Taipei	VPRE (hPa)	28	29	29.5	28.5	28.5
	HUMD (%)	70.5	65.5	59	56	54
	WDIR (°)	140–200	180–210	230–280	230–330	260–350
	WDSD (m s^{-1})	<1.5	<1.5	<2.0	<2.0	<2.5
Sounding, 0800 LST	hPa	1000	925	850	700	500
Panchiao	CAPE (m^2 s^2)			>500		
	$T - T_d$ (°C)	<4.0	<4.0	<6.0	<9.5	<11.0
	WDIR (°)	210	230–280	220–280	200–270	200–250
	WDSD (m s^{-1})	<1.5	<4.0	<4.5	<6.5	<6.5

Lin et al. (2012)

In this step, the values from individual membership functions for a given day are weighted and summed to produce a likelihood value (Y_s) for that day (TS_A and non-TS_A days). This is expressed by the equation below:

$$Y_s = \frac{\sum L_{k,s}(x_k) \times W_{k,s}}{\sum W_{k,s}},$$

where $L_{k,s}(x_k)$ is the likelihood of membership function for each predictor x_k and its $W_{k,s}$ is the membership function weight for type s (TS_A and non-TS_A day). For each day, each of the 28 membership functions and the persistence rule were weighted and summed to obtain the final likelihood value Y_s (steps 5–8 in Fig. 3). In other words, the forecast of TS_A is obtained by converting the predictors to dimensionless likelihood values using the membership functions shown in Fig. 6, weighting the importance of each likelihood value to the forecast, and summing. The likelihood value of TS_A varies from 0 to 1. For this study we used a likelihood value >0.5 as a forecast for a TS_A day.

Lin et al. (2012)

當決定每一個預報因子的隸屬函數〔$L_{k,s}(X_k)$，圖 9〕，經由其所具有的權重($W_{k,s}$)，累加其經權重化後所得之可能發生機率，便可得當天可能發生的 TS_A 機率值(Y_s)，可表示為：

$$Y_s = \frac{\sum L_{k,s}(x_k) \times W_{k,s}}{\sum W_{k,s}}$$

在本研究中，28 個預報因子及持續性將經由上式計算在弱綜觀環境下的每一天，其 TS_A 可能發生的機率，當 $Y_s > 0.5$，將預報會有 TS_A 發生。而權重的決定則是每一個預報因子皆由 0–1，間隔 0.1 進行 CSI 技術得分（或可稱為 threat score, TS; Bermowitz and Zurndorfer 1979）的計算，以最大 CSI 值時之各權重為其各項預報因子的權重，並用來評估 ATOPFLO 預報之能力。另外兩

林等 (2012；大氣科學)

Lin et al. (2012)

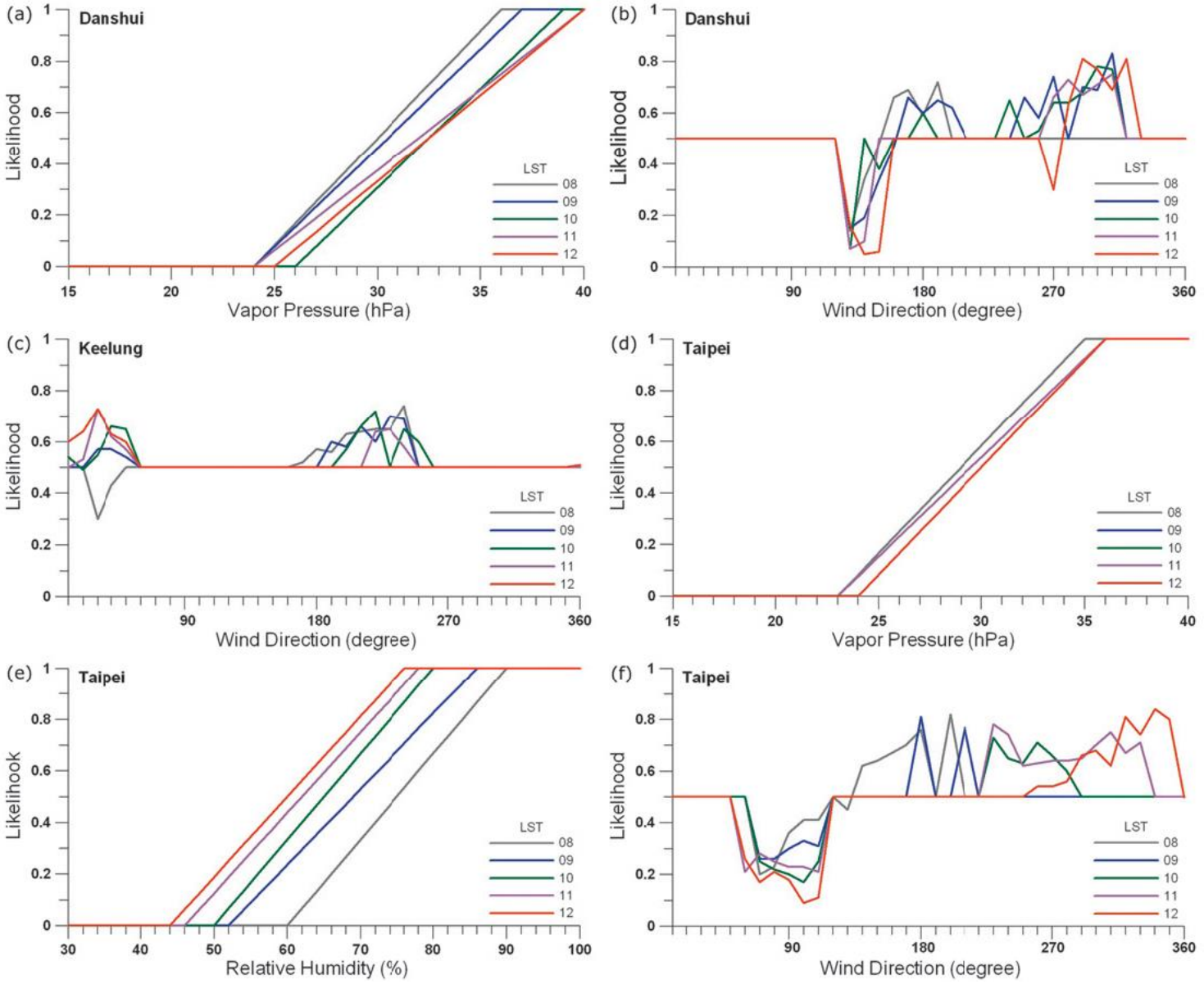

FIG. 6. Fuzzy membership functions corresponding to the TS_A days derived from the conditional probability curves in Fig. 5.

Lin et al. (2012)

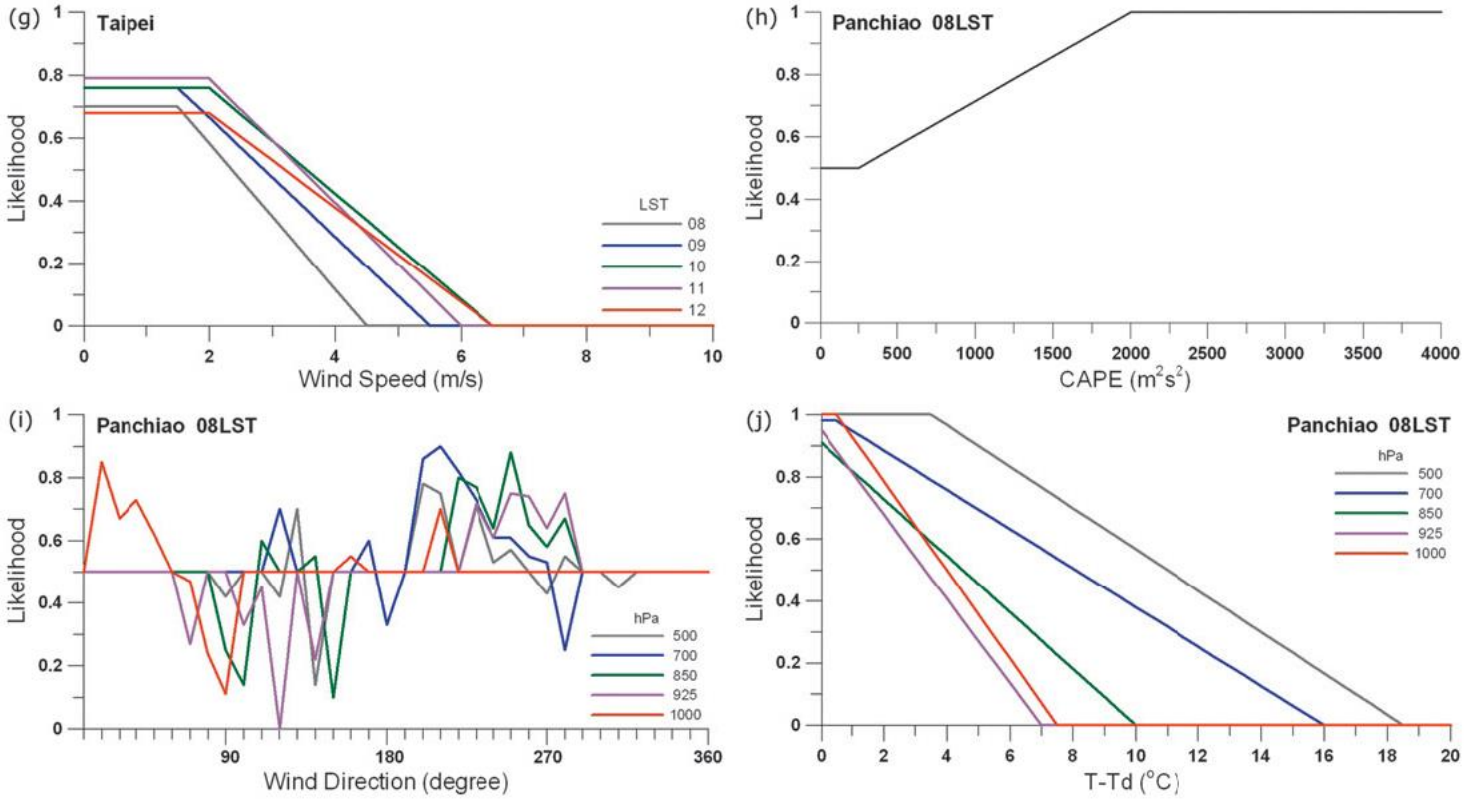

FIG. 6. Fuzzy membership functions corresponding to the TS_A days derived from the conditional probability curves in Fig. 5.

TABLE 4. Hourly weights of surface station predictors for the occurrence of TS_As and associated CSI values obtained from the fuzzy logic approach. Predictors with higher weights are set in boldface.

Station	Hour (LST)	0800	0900	1000	1100	1200
Danshui	VPRE (hPa)	**0.171**	**0.136**	0.020	**0.143**	**0.171**
	HUMD (%)	0.026	0.0	0.0	0.0	0.082
	WDIR (°)	0.051	**0.097**	**0.097**	**0.196**	**0.140**
	WDSD (m s^{-1})	**0.188**	**0.113**	**0.099**	0.041	**0.110**
Keelung	VPRE (hPa)	0.034	0.030	0.044	0.013	0.038
	HUMD (%)	0.004	0.0	0.0	0.0	0.057
	WDIR (°)	0.008	**0.111**	**0.226**	0.0	0.0
	WDSD (m s^{-1})	0.047	0.075	**0.127**	**0.136**	**0.099**
Taipei	VPRE (hPa)	0.088	0.083	**0.097**	**0.157**	**0.093**
	HUMD (%)	0.059	**0.167**	**0.097**	**0.137**	0.047
	WDIR (°)	0.059	0.042	**0.161**	0.020	0.023
	WDSD (m s^{-1})	**0.265**	**0.146**	0.032	**0.157**	**0.140**
	CSI	**0.682**	**0.690**	**0.703**	**0.722**	**0.726**

Lin et al. (2012)

TABLE 5. As in Table 4, but for sounding predictors.

Sounding, 0800 LST	hPa	1000	925	850	700	500
Panchiao	CAPE (m^2 s^2)			**0.210**		
	$T - T_d$ (°C)	**0.291**	0.036	0.036	0.036	**0.073**
	WDIR (°)	0.033	0.038	**0.057**	0.033	**0.051**
	WDSD (m s^{-1})	**0.077**	0.0	0.0	0.0	0.029
	CSI			**0.702**		

$$\mathrm{CSI} = \frac{h}{(h + m + f)}, \quad \mathrm{POD} = \frac{h}{(h + m)},$$

$$\mathrm{FAR} = \frac{f}{(h + f)},$$

where h, m, and f are defined as hits, misses, and false alarms, respectively. The hits and misses represent correct and incorrect predictions, while days incorrectly considered as TS_A days are false alarms.

Lin et al. (2012)

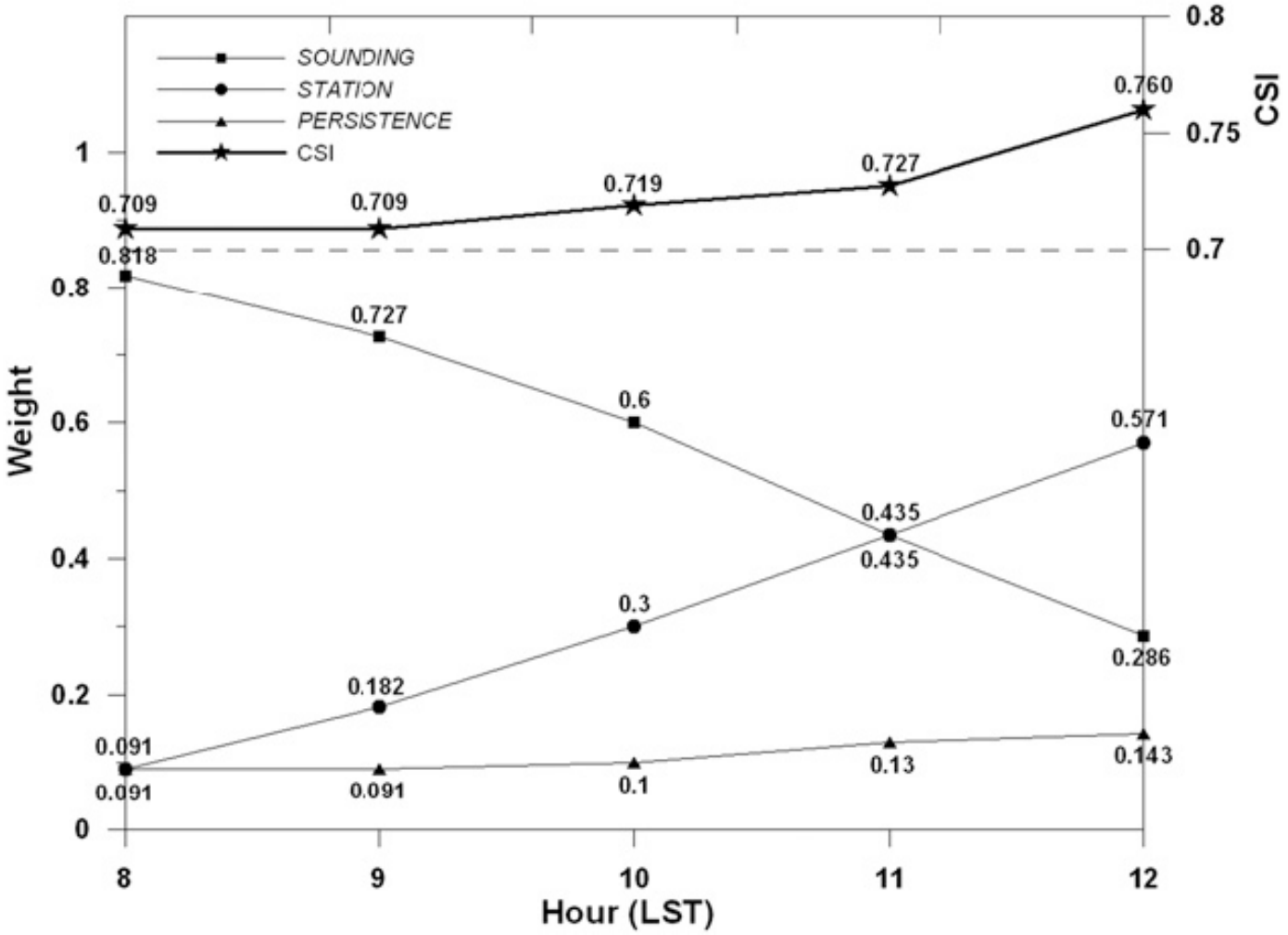

FIG. 7. Fuzzy weights for each hour forecast for predictors STATION, SOUNDING, and PERSISTENCE. The corresponding CSI value for forecasting a TS_A day is given at the top of the figure (note the CSI scale at the top right).

Lin et al. (2012)

TABLE 6. Hourly skill scores of the fuzzy logic algorithm and CWB forecasters for the calibration dataset (May–October 2005–08).

	Time (LST)	Hit	Miss	False alarm	Correct rejection	POD	FAR	CSI
	0800	134	14	41	86	0.905	0.234	0.709
	0900	134	14	41	86	0.905	0.234	0.709
Fuzzy	1000	133	15	37	90	0.899	0.218	0.719
	1100	136	12	39	88	0.919	0.223	0.727
	1200	136	12	31	96	0.919	0.186	0.760
CWB	1030	124	24	58	69	0.838	0.319	0.602

Lin et al. (2012)

TABLE 7. As in Table 6, but for the validation dataset (May–October 2009–10).

	Time (LST)	Hit	Miss	False alarm	Correct rejection	POD	FAR	CSI
	0800	40	5	27	46	0.889	0.403	0.556
	0900	39	6	27	46	0.867	0.409	0.542
Fuzzy	1000	39	6	25	48	0.867	0.391	0.557
	1100	39	6	21	52	0.867	0.350	0.591
	1200	38	7	19	54	0.844	0.333	0.594
CWB	1030	35	10	29	44	0.778	0.453	0.473

Lin et al. (2012)

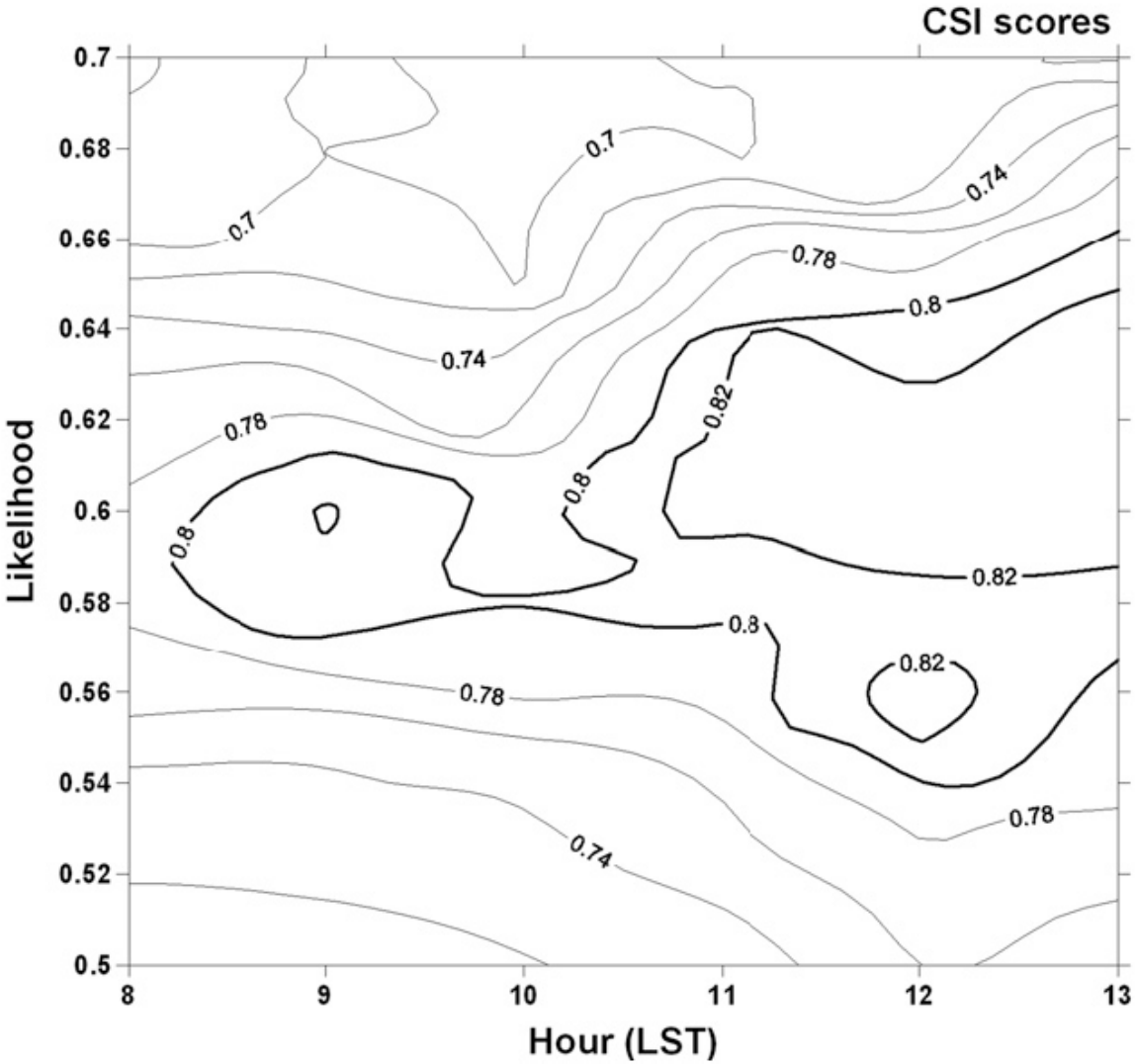

FIG. 8. CSI scores for forecasting the occurrence of TS_As as a function of the time of the forecast (h) and threshold value (Y_s, likelihood) for declaring a TS_A day. Contours indicate the CSI values; values ≥0.8 are indicated with heavy lines.

Lin et al. (2012)

The synoptic environment for a TS_A day

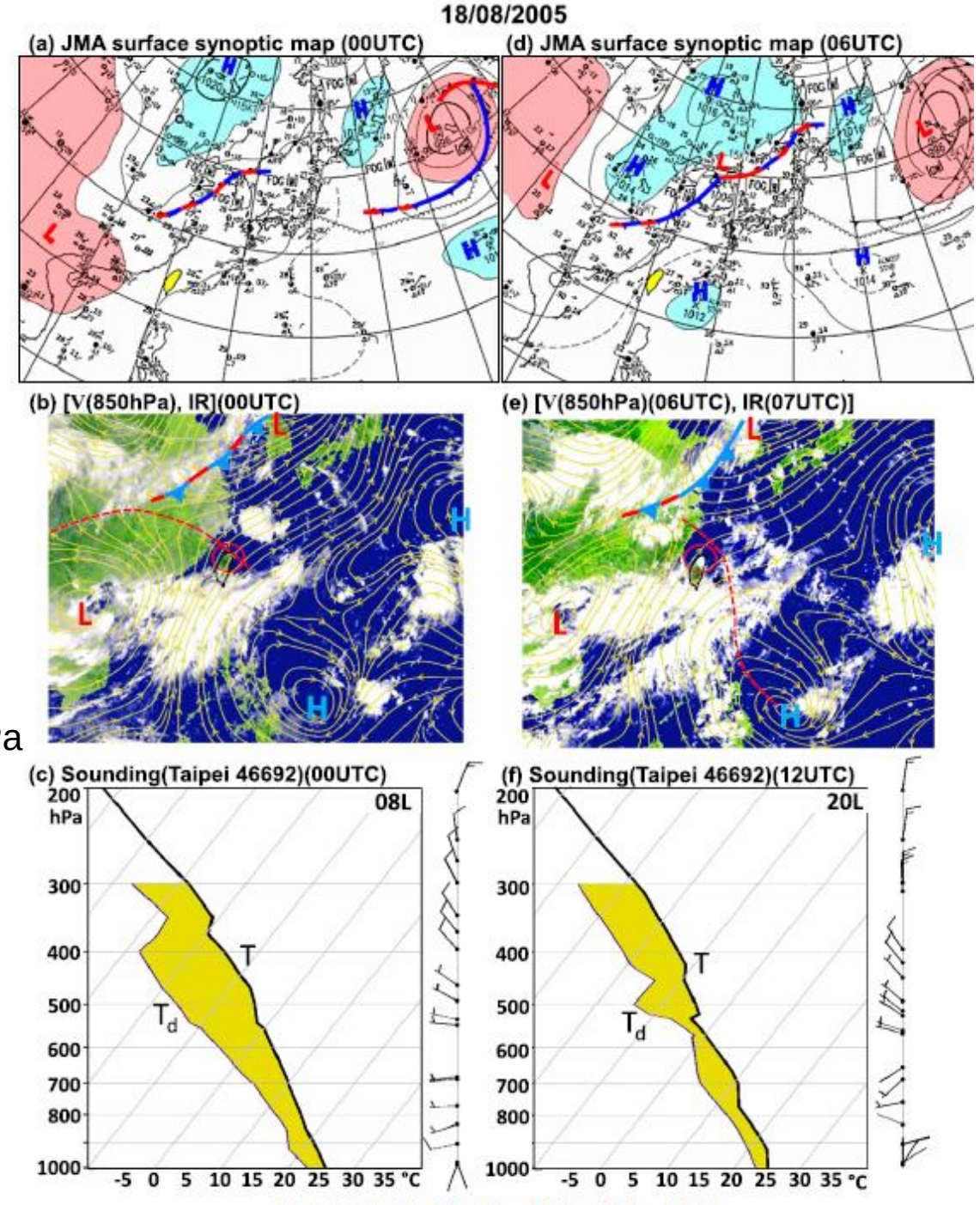

FIG. 7. As in Fig. 4, but for a TS day (18 Aug 2005).

⇒ Prevailing SW flow at 850 hPa
⇒ Moisture at low-to-mid levels

Chen et al. (2014)

Evolution of radar echo at 3-km level for a TS_A day

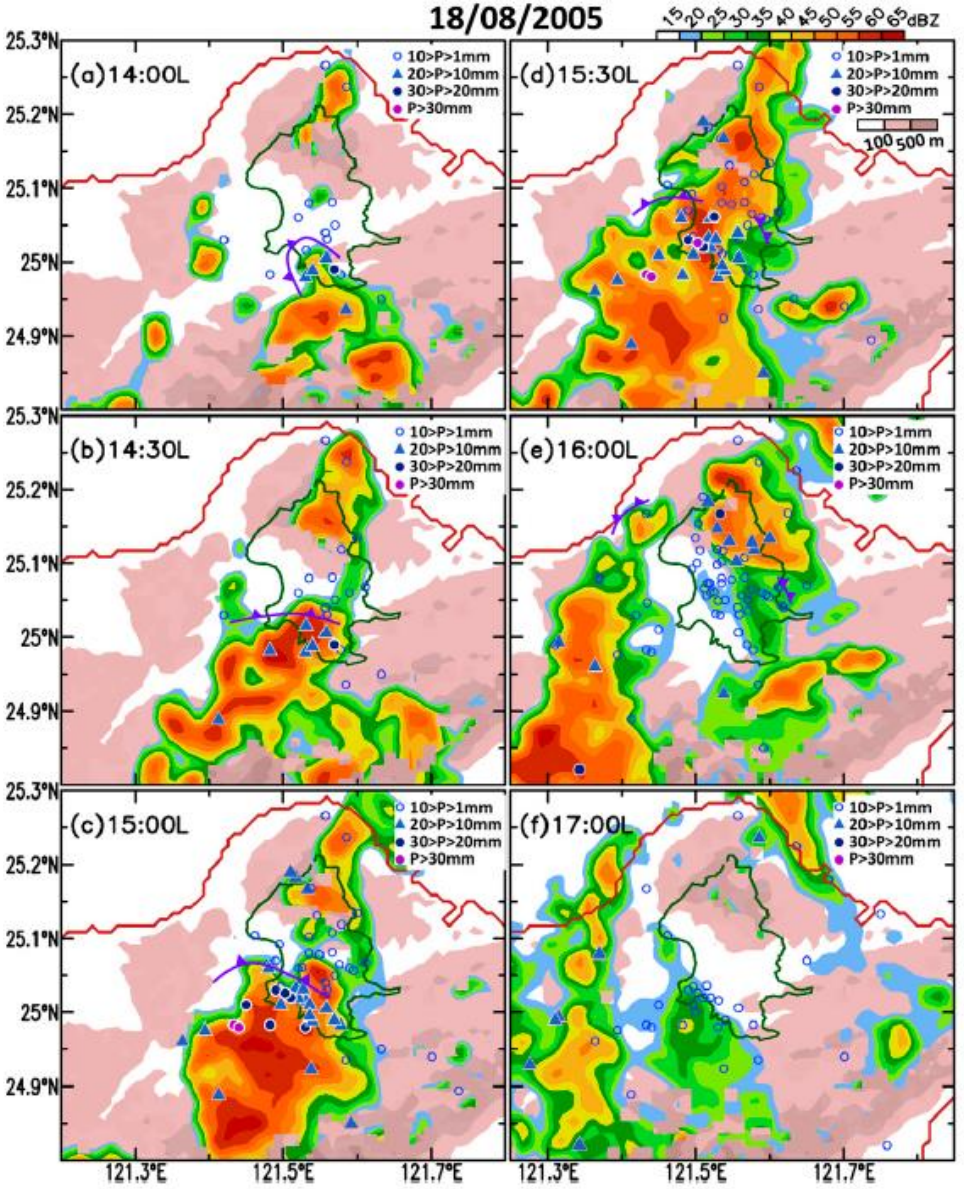

FIG. 10. The radar echo on 18 Aug 2005 (a TS day) at an altitude of 3 km, superimposed with half-hour rainfall accumulation measured by surface stations, is used to depict the TS convection/rainfall over the life cycle of that afternoons' thunderstorms. The rainfall amount is colored by symbols shown in the top-right corner of each panel. The color scale of the radar echo (1 km × 1 km resolution) is shown on the top right of the figure. The surface front ahead of the surface mesohigh is determined as in Fig. 9. The selection of the 3-km radar echo is based on the following reasoning: The vertical profile of the radar echo (supplement 9) over its maximum area southwest of the Taipei district shows that the maximum echo is located in the 3–5-km layer; the distribution of the rainfall measurement by surface stations within the Taipei basin and its surrounding areas matches best with the 3-km radar echo.

Chen et al. (2014)

$$\Delta T_d = T - T_d$$

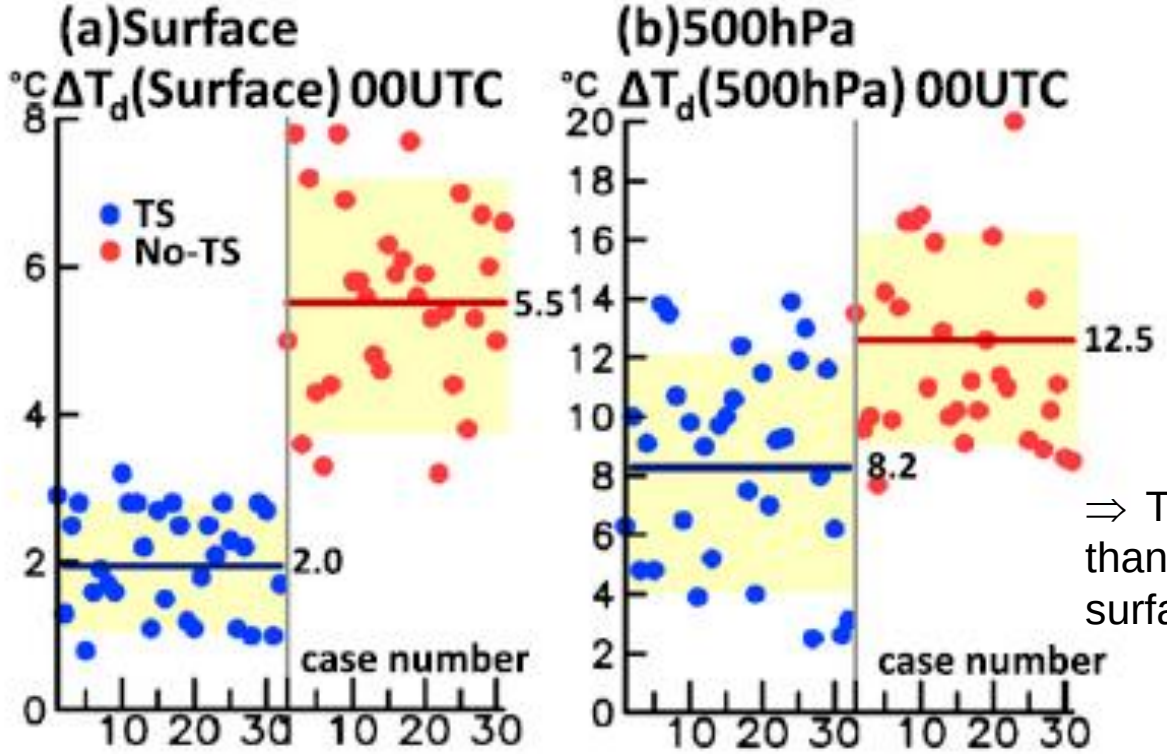

⇒ The air of a TS_A day is moister than that of a non-TS_A day, for both surface and 500-hPa

Chen et al. (2014)

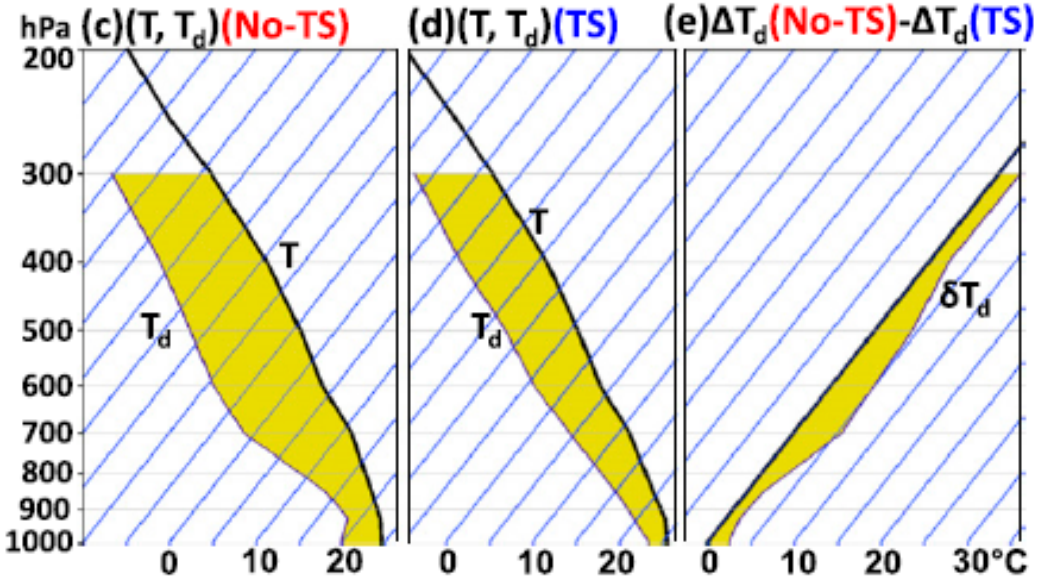

FIG. 11. The 0000 UTC radiosonde measurements of T and T_d at Taipei (WMO 46692): scatter diagrams of ΔT_d ($=T - T_d$) on the ordinate vs case number on the abscissa at (a) the first sounding level (60 m) and (b) 500 hPa for both TS days (blue dots) and no-TS days (red dots) and composite vertical profiles of (c),(d) T and T_d for no-TS and TS days, respectively, and (e) ΔT_d(no-TS) $-$ ΔT_d(TS) $= \delta T_d$. Standard deviations σ of ΔT_d(no-TS) and ΔT_d(TS) are shown by yellow shading in (a) and (b); composites of ΔT_d(no-TS), ΔT_d(TS), and δT_d are indicated by golden shading in (c)–(e). The two-tailed t test is applied to test whether both groups of ΔT_d(TS) and ΔT_d(no-TS) are statistically different from each other. Results of this t test are the p

$$\Delta T_d(\text{no-TS}) - \Delta T_d(\text{TS}) = \delta T_d.$$

The composite soundings of 33 non-TS_A days and 32 TS_A days
$\Rightarrow$ The sounding for TS_A days is much moister than that for non-TS_A days, and the result is statistically significant.

Chen et al. (2014)

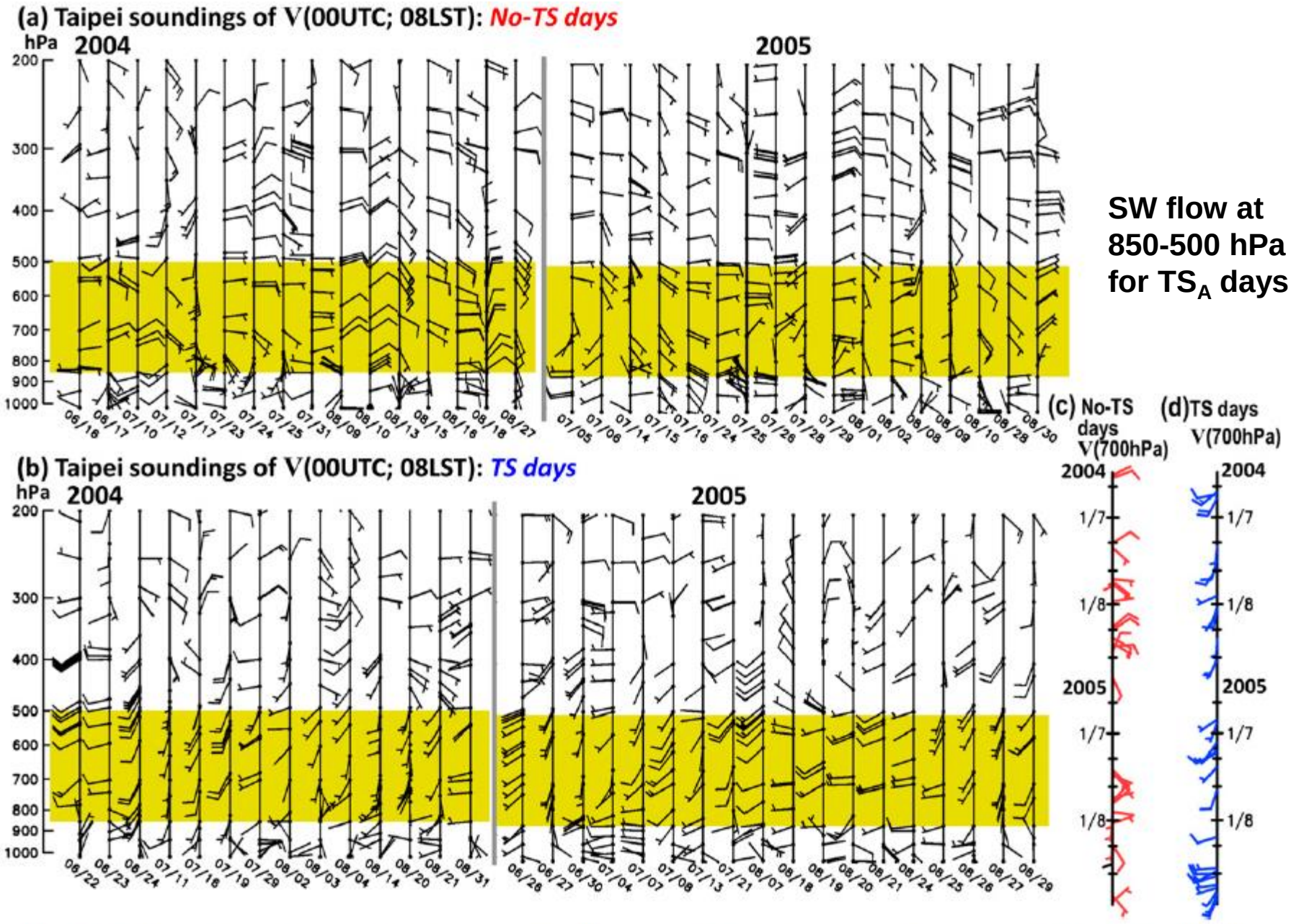

FIG. 12. The Taipei V soundings at 0000 UTC for (a) 33 no-TS days and (b) 32 TS days over the summers of 2004 and 2005. The lower-tropospheric monsoon flows at Taipei are shown by the V soundings over the 850–500-hPa layer marked with a golden stripe. To show the directional

Chen et al. (2014)

TABLE 5. Onset and cessation time and life span of the sea breezes at the valley exit stations (lightface font) and stations close to mountain slopes (boldface font) along the Tanshui and Keelung River valleys.

River valley	Type	Station	Onset time (LST)	Cessation time (LST)	Duration
Tanshui	No TS	Tanshui	0958	1855	8 h, 57 min
		Jin-mei	**1204**	**1818**	**6 h, 14 min**
	TS	Tanshui	0956	1634	6 h, 38 min
		Jin-mei	**1026**	**1442**	**4 h, 16 min**
Keelung	No TS	Keelung	0950	1852	9 h, 02 min
		Panchao	**1205**	**1815**	**6 h, 10 min**
	TS	Keelung	0956	1648	6 h, 52 min
		Panchao	**1032**	**1450**	**4 h, 18 min**

$\Rightarrow$ For a TS_A day, the duration of sea breeze is shorter than that for the a non-TS_A day.
$\Rightarrow$ In particular, for a TS_A day, the sea breeze ends at a earlier time than that for a non-TS_A day.

Chen et al. (2014)

The sea breeze onset and ending times at the valley exit and mountain slope stations for the Tanshui river valley

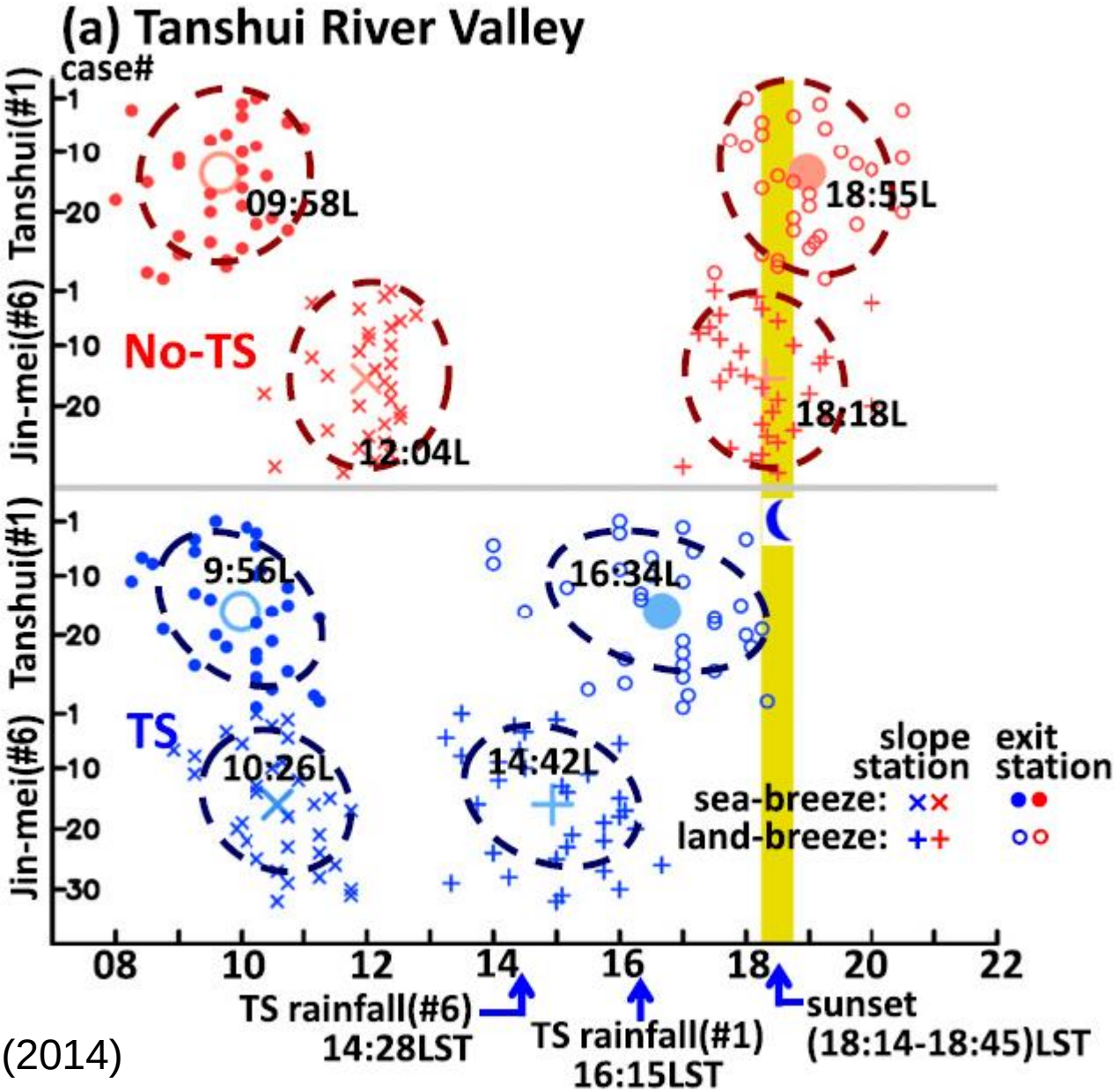

Chen et al. (2014)

The sea breeze onset and ending times at the valley exit and mountain slope stations for the Keelung river valley

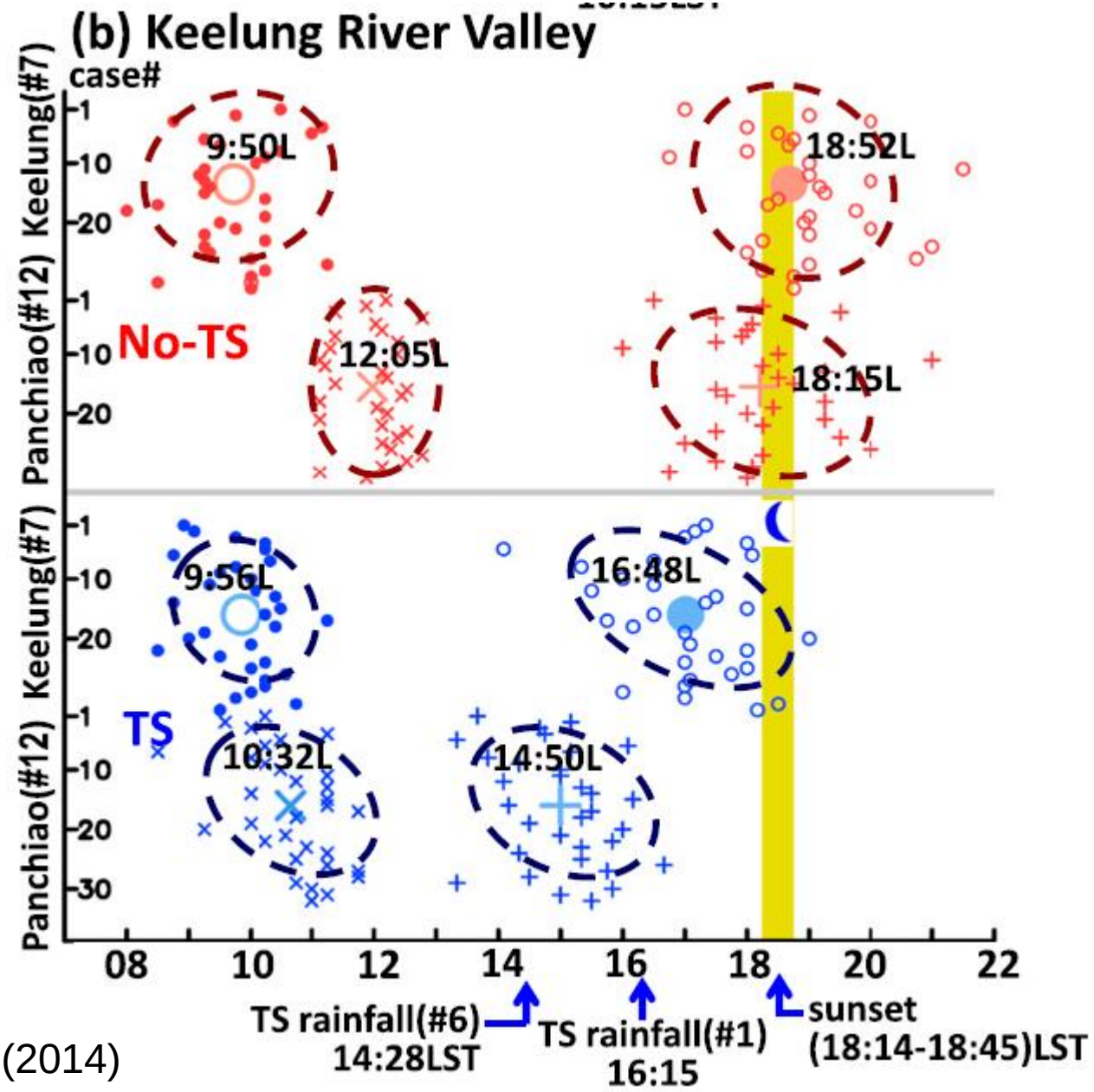

Chen et al. (2014)

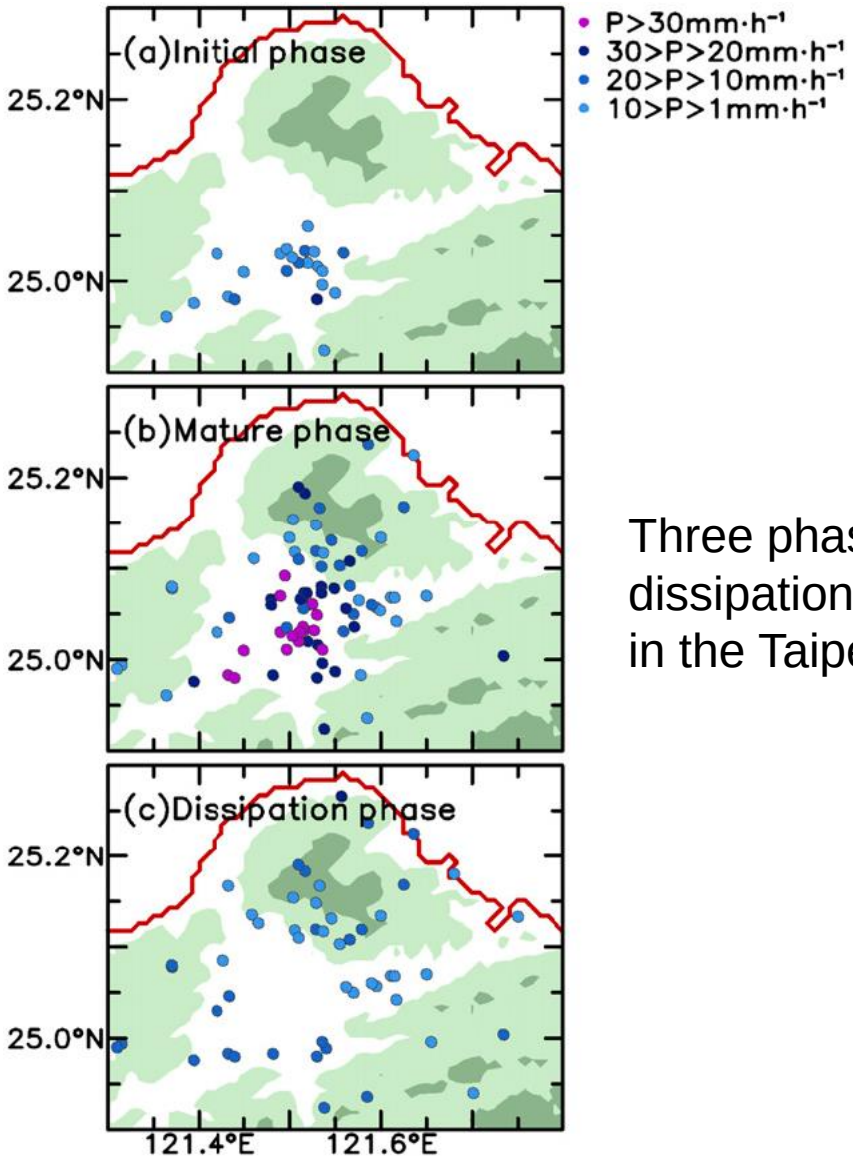

Three phases (initial, mature, and dissipation) of afternoon thunderstorm in the Taipei basin in terms of rainfall rate

Chen et al. (2014)

FIG. 18. Composite life cycle of afternoon thunderstorms in the Taipei basin depicted with station rainfall measurements over the TBEX domain (Fig. 2). The afternoon thunderstorm life cycle is depicted with 30-min rainfall accumulations. As long as the life

Conclusions (I)

- The highest frequency of TS_A occurred along the lower mountain slopes along the ridges of the SMR and CMR.

- TS_A occurred earlier in northern Taiwan, but the TS_A activity lasted longer in central and southern Taiwan.

- The mean T and Td profiles at low-to-middle levels were relatively warmer and moister on TS_A days than non-TS_A days.

- The wind flows in the 0-6 km layers for the TS_A days are the humid southwesterly flows.

Conclusions (II)

- The local trigger for TS_A is the convergence of moist sea breeze into the Taipei Basin from the Tanshui and Keelung river valleys.

- Membership functions and weights were developed for 28 predictors from 3 CWB surface stations (Danshui, Keelung, and Taipei) and the Panchiao sounding, and the persistence of TS_A from previous day was the 29^{th} predictor.

- The weighting of the 08 LST sounding decreases as the day progresses, and the weighting of surface stations increases with time.

- If the sounding conditions are generally favorable, the local circulations such as sea breeze and wind convergence line determine the location and timing for TS_A.

Thank you for listening

Warm Season Afternoon Thunderstorm Characteristics under Weak Synoptic-Scale Forcing over Taiwan Island

PIN-FANG LIN

Department of Atmospheric Sciences, National Taiwan University, and Central Weather Bureau, Taipei, Taiwan

PAO-LIANG CHANG

Central Weather Bureau, Taipei, Taiwan

BEN JONG-DAO JOU

Department of Atmospheric Sciences, National Taiwan University, Taipei, Taiwan

JAMES W. WILSON AND RITA D. ROBERTS

National Center for Atmospheric Research, Boulder, Colorado

(Manuscript received 24 November 2009, in final form 4 July 2010)

Objective Prediction of Warm Season Afternoon Thunderstorms in Northern Taiwan Using a Fuzzy Logic Approach

PIN-FANG LIN AND PAO-LIANG CHANG

Central Weather Bureau, Taipei, Taiwan

BEN JONG-DAO JOU

Department of Atmospheric Sciences, National Taiwan University, Taipei, Taiwan

JAMES W. WILSON AND RITA D. ROBERTS

National Center for Atmospheric Research, Boulder, Colorado

(Manuscript received 21 September 2011, in final form 29 March 2012)

Impact of Afternoon Thunderstorms on the Land–Sea Breeze in the Taipei Basin during Summer: An Experiment*

TSING-CHANG CHEN

Department of Geological and Atmospheric Sciences, Iowa State University, Ames, Iowa

MING-CHENG YEN

Department of Atmospheric Sciences, National Central University, Chung-Li, Taiwan

JENQ-DAR TSAY

Department of Geological and Atmospheric Sciences, Iowa State University, Ames, Iowa

CHI-CHANG LIAO

Department of Environmental Information and Engineering, Chung-Cheng Institute of Technology, National Defense University, Taoyuan, Taiwan

EUGENE S. TAKLE

Department of Geological and Atmospheric Sciences, and Department of Agronomy, Iowa State University, Ames, Iowa

(Manuscript received 11 March 2013, in final form 10 February 2014)

Two paths of sea breeze along two river valleys into the Taipei basin

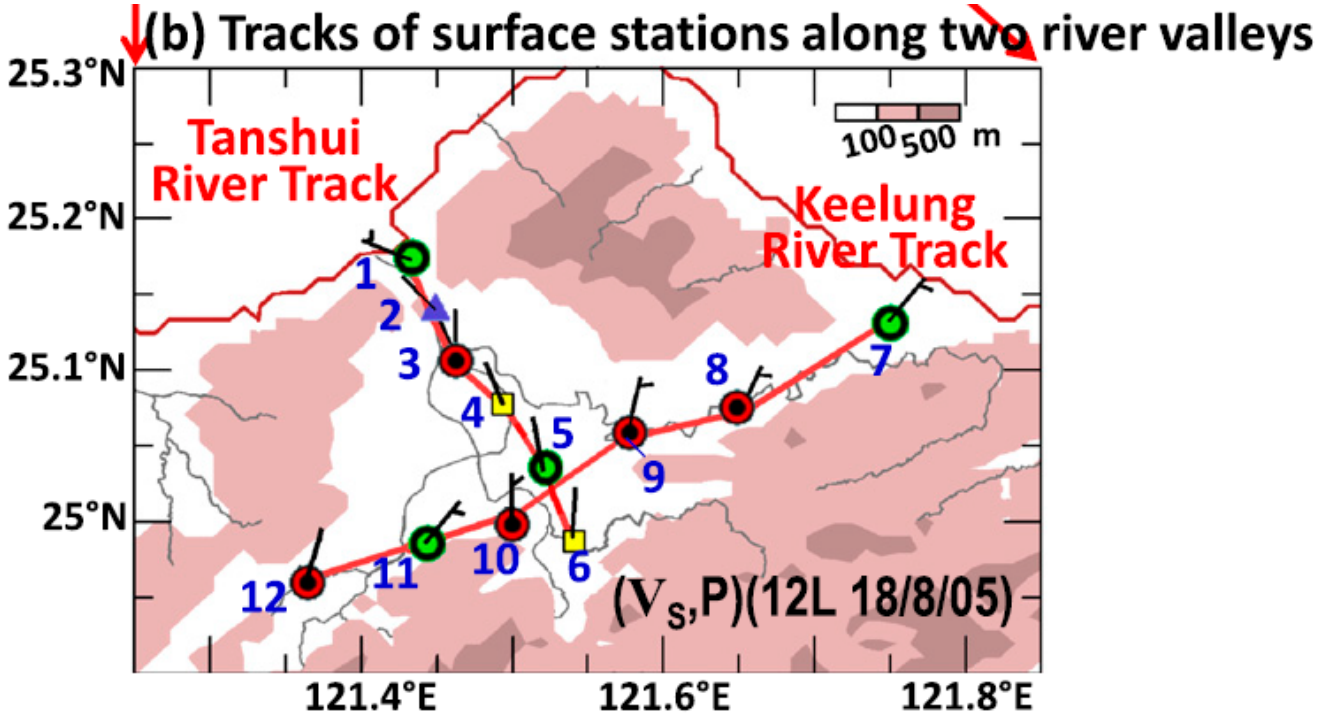

FIG. 2. Observational network used for TBEX during the summers of 2004 and 2005. (a) Surface and radiosonde stations, radars, and satellites provided by different agencies and supplemented by seven TBEX AWOS and two mobile radiosonde stations at Tanshui and Keelung. Networks for radiosonde, radar, and WMO surface stations in Taiwan are shown in the small panel in the bottom-right corner. (b) Two tracks of surface stations connected by red lines along the Taishui (1–6) and Keelung (7–12) River valleys. Time series of meteorological variables measured at these stations will be used to depict diurnal variations of meteorological conditions along these two river valleys. Surface winds measured at 1500 LST 28 Jul 2005 are displayed to illustrate the sea breezes along these valleys. The topography (m) is included in each panel.

Chen et al. (2014)

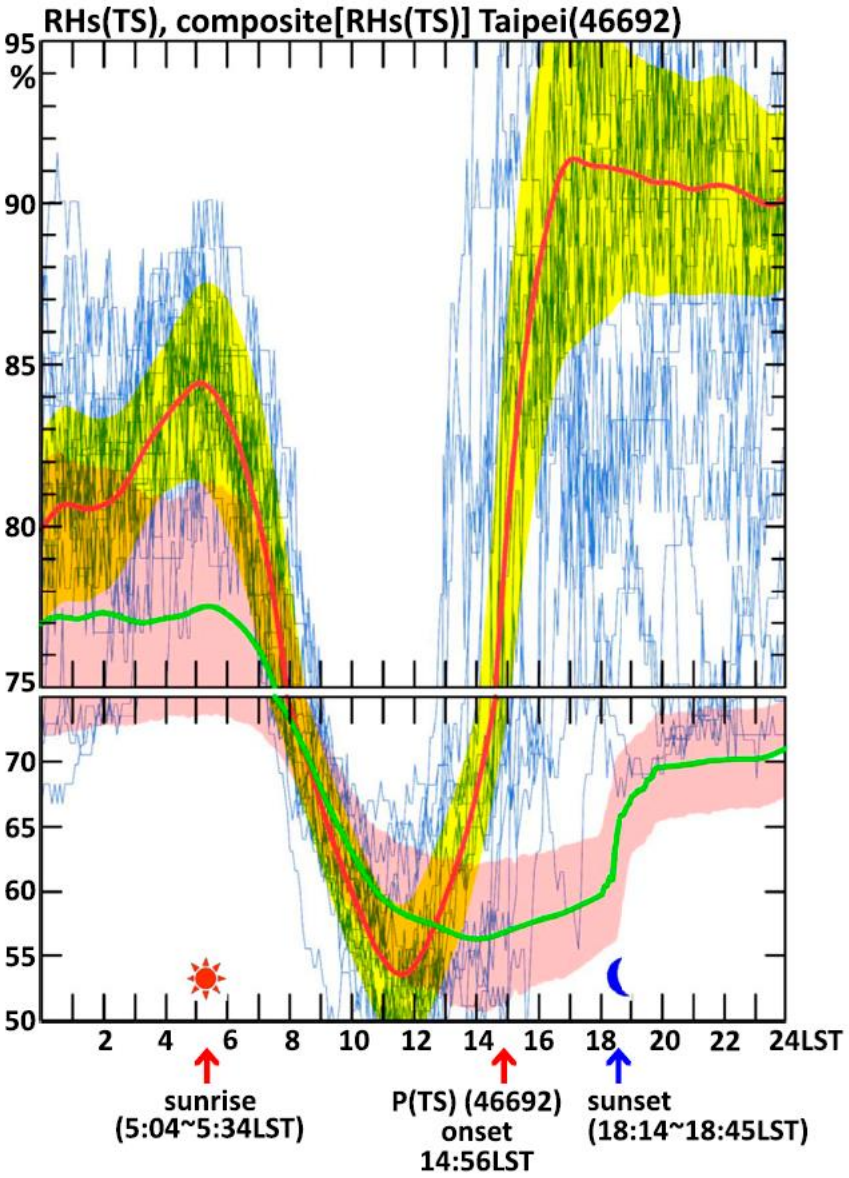

FIG. 16. Composite RH_s(TS) time series at Taipei (WMO 46692) for 32 TS days (thick red line) superimposed with 1σ (yellow shading). The real-time RH_s(TS) time series for each individual TS day is portrayed by the thin blue line. The composite RH_s(no TS) time series for the 33 no-TS days (thick green line) superimposed with 1σ (pink shading) is also added for reference. The sunrise and

Time series of composite RH for TS_A day (red line) and for non-TS_A day (green line)

Chen et al. (2014)